NASA TECHNICAL NOTE

NASA TN D-2184

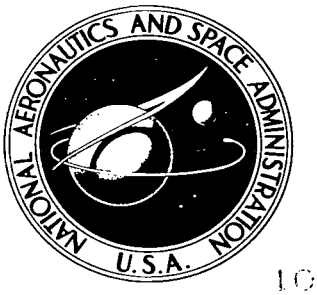

NASA TN D-2184

FORCE-COEFFICIENT AND MOMENT-COEFFICIENT CORRELATIONS AND AIR-HELIUM SIMULATION FOR SPHERICALLY BLUNTED CONES

by Julius E. Harris

Langley Research Center
Langley Station, Hampton, Va.

NATIONAL AERONAUTICS AND SPACE ADMINISTRATION • WASHINGTON, D. C. • NOVEMBER 1964

FORCE-COEFFICIENT AND MOMENT-COEFFICIENT CORRELATIONS AND AIR-HELIUM SIMULATION FOR SPHERICALLY BLUNTED CONES

By Julius E. Harris

Langley Research Center
Langley Station, Hampton, Va.

NATIONAL AERONAUTICS AND SPACE ADMINISTRATION

For sale by the Office of Technical Services, Department of Commerce,
Washington, D.C. 20230 -- Price $1.25

FORCE-COEFFICIENT AND MOMENT-COEFFICIENT CORRELATIONS AND AIR-HELIUM SIMULATION FOR SPHERICALLY BLUNTED CONES*

By Julius E. Harris
Langley Research Center

SUMMARY

An experimental force and moment investigation has been conducted in air, nitrogen, and helium on a family of 10° semiapex angle cones with various bluntness ratios. The tests were made in three hypersonic facilities at the NASA Langley Research Center. The investigation covered a range of Mach numbers from 9.75 to 19.15 and Reynolds numbers from 0.75×10^5 to 6.12×10^5 for angles of attack from 0° to 45°.

Analysis of the data from the present investigation together with data from previous investigations for other cone angles indicates that a correlation of normal-force and pitching-moment coefficients could be made as a function of body geometry and angle of attack for slender cones having small to moderate bluntness ratios.

The data obtained in air and nitrogen were nearly duplicated in helium for the test conditions of Mach number, Reynolds number, and body geometry studied.

Newtonian impact theory was found to predict the trends of the aerodynamic characteristics, and in many instances quite accurately predicted the actual magnitudes of the force and moment coefficients.

INTRODUCTION

It is highly desirable to be able to predict with reasonable accuracy the force and moment coefficients for any member of a class of geometrically similar bodies once these characteristics are known for any one member of the class. A method for correlating normal-force and pitching-moment coefficients for spherically blunted cones as a function of body geometry and angle of attack is presented in references 1 and 2. However, the major portion of the experimental

*The information presented herein is based in part upon a thesis entitled "A Basic Study of Spherically Blunted Cones Including Force and Moment Coefficient Correlations and Air-Helium Simulation Studies" submitted by Julius E. Harris in partial fulfillment of the requirements for the degree of Master of Science in Aerospace Engineering, Virginia Polytechnic Institute, Blacksburg, Virginia, March 1964.

data presented in these references was obtained during viscous interaction studies on slightly blunted slender cones over a limited angle-of-attack range. Consequently, these data have not clearly established the effects of increasing cone angle, bluntness ratio, and angle of attack on the correlation.

There is a continuing interest in the use of helium facilities to study the aerodynamic characteristics of hypersonic configurations. It is important to know for all aerodynamic studies in helium whether adequate air-helium simulation can be achieved, or whether helium data can be suitably transformed to equivalent air data. For a wide range of test conditions in both air and helium an ideal gas can be assumed. Consequently, the primary difference between air and helium is the ratio of specific heats. The simulation of aerodynamic data by the use of helium as a test medium has received considerable attention in theoretical work. (See refs. 3 to 5.) There have also been a few studies where specific configurations have been tested in air and helium and the experimental data compared. However, in general, these comparisons have dealt with lifting bodies and pointed cones. (See refs. 6 to 11.)

Newtonian impact theory provides one of the simplest, yet most useful, means of estimating the aerodynamic characteristics of complete or partial conic and spheric bodies at hypersonic speeds, and in many instances is the only practical theory available. (See refs. 12 to 14.)

The purpose of the present investigation was threefold: (1) to study and improve, where possible, existing force-coefficient and moment-coefficient correlations, (2) to compare data obtained in helium, air, and nitrogen and from this comparison to determine the validity of using data obtained in helium facilities for spherically blunted cones, and (3) to study the aerodynamic characteristics of spherically blunted cones and to determine the adequacy of Newtonian impact theory for predicting these characteristics.

SYMBOLS

A area, sq ft

C_A axial-force coefficient, $\frac{F_A}{q_\infty A_b}$

C_D drag coefficient, $\frac{F_D}{q_\infty A_b}$

C_L lift coefficient, $\frac{F_L}{q_\infty A_b}$

C_m pitching-moment coefficient, $\frac{M}{q_\infty A_b d}$

C_N	normal-force coefficient, $\frac{F_N}{q_\infty A_b}$
C_p	pressure coefficient, $\frac{p - p_\infty}{q_\infty}$
d	cone base diameter, ft
F_A	axial force, lb
F_D	drag force, $\left(F_N \sin \alpha + F_A \cos \alpha\right)$, lb
F_L	lift force, $\left(F_N \cos \alpha - F_A \sin \alpha\right)$, lb
F_N	normal force, lb
L	length of model, ft
L_1, L_2	defined in figure 4, ft
L/D	lift-drag ratio, $\frac{C_L}{C_D}$
M	pitching moment, ft-lb
M_∞	free-stream Mach number
p	pressure, lb/sq ft
q	dynamic pressure, $\frac{1}{2}\rho V^2$, lb/sq ft
R	Reynolds number, $\frac{\rho_\infty V_\infty d}{\mu_\infty}$
r	radius, ft
T	temperature, $^\circ R$
V	velocity, ft/sec
X	longitudinal body axis
x	distance along X-axis (see fig. 4)
$\bar{x}$	distance to centroid of planform area, ft
α	angle of attack, deg

$\alpha_{(L/D)_{max}}$ angle of attack for maximum lift-drag ratio, deg

γ ratio of specific heats

θ defined in figure 4, deg

ρ density, slugs/ft^3

ϕ cone semiapex angle, deg

ψ bluntness ratio, $\frac{r_n}{r_b}$

μ coefficient of viscosity, $\frac{\text{lb-sec}}{\text{ft}^2}$

Subscripts:

approx approximate

b base

c cone

m point of tangency between spherical nose and conical body

max maximum

n nose

p planform

$\bar{p}$ planform neglecting spherical nose

s sphere

t total conditions ahead of normal shock

w windward

∞ free stream

1,2,3,4 defined in figure 4

TEST FACILITIES

The present investigation was conducted in three hypersonic research facilities at the NASA Langley Research Center: the Langley hotshot tunnel, the

Langley 11-inch hypersonic tunnel, and the Langley 22-inch helium tunnel. These facilities are discussed briefly in the following paragraphs.

The Langley hotshot tunnel is an arc-heated, hypervelocity blowdown tunnel. Nitrogen was used as the test medium for the present investigation. The major components include a capacitor bank for storage of electrical energy, an arc-heated reservoir, a 10° conical nozzle, a 24-inch-diameter cylindrical test section, a diffuser, and a 300-cubic-foot vacuum chamber. A sketch of the facility is presented in figure 1.

The operation of the facility for the present investigation was as follows: First, the tunnel and vacuum chamber were pumped down to approximately 10 microns of mercury and the arc chamber was pressurized to 1000 psia at room temperature. Next, the capacitor storage system was charged to the desired energy level and then discharged into the arc chamber. The arc heated and pressurized the nitrogen to approximately 5000° R and 11,000 psia. The high-pressure nitrogen then ruptured a diaphragm separating the arc chamber from the nozzle and expanded through the conical nozzle to a Mach number of approximately 19 in the test section. Once the desired data were obtained, the run was terminated by exhausting the nitrogen remaining in the arc chamber through a dump valve. A more thorough description of the facility and its operation is presented in reference 15.

The Langley 11-inch hypersonic tunnel is an intermittent closed-cycle tunnel designed to operate with air as the test medium for Mach numbers of approximately 7 and 10. A thorough description of the facility is presented in reference 16. Since reference 16 was published, the storage heater has been replaced by an electric heater and the tunnel now has invar nozzle blocks which have reduced the test-section Mach number variations with time resulting from warpage at the nozzle throat. (See ref. 17.)

The Langley 22-inch helium tunnel is an intermittent closed-cycle tunnel. A description of the facility and its operation is presented in reference 18. A tunnel calibration for the contoured nozzle used in the present investigation is presented in reference 8.

TEST CONDITIONS

The approximate test conditions for the present investigation are listed in the following table:

Parameter	Langley 11-inch hypersonic tunnel	Langley hotshot tunnel	Langley 22-inch helium tunnel
γ	7/5	7/5	5/3
M_∞	9.75	19.15	19.15
R	1.56×10^5	0.75×10^5	6.12×10^5
p_t, psia	662	11,000	520
T_t, °R	1711	5000	555
p_∞, psia	0.018	0.002	0.003
T_∞, °R	85.6	87	4.5

INSTRUMENTATION

Internally mounted strain-gage balances were used to measure the forces and moments in the three test facilities. Angles of attack were set in the Langley 11-inch hypersonic tunnel and the Langley 22-inch helium tunnel during the tunnel run by using a prism mounted in the model to reflect the light from a point source outside the tunnel onto a calibrated scale. In the 22-inch helium tunnel the light was reflected onto photoelectric cells which were set at the desired angle-of-attack intervals. As the reflected light beam swept past each cell, an electrical relay was energized and caused a high-speed digital recorder to sample and record the strain-gage outputs on magnetic tape. In the 11-inch hypersonic tunnel the angles of attack were set manually by positioning the reflected light beam on a calibrated scale. The strain-gage outputs were recorded on strip-chart recorders. The angle of attack was not changed during a test run in the Langley hotshot tunnel because of the short duration of test time. Strain-gage outputs were amplified by a 3-kc system and recorded on an oscillograph.

Thermocouples and pressure transducers were used to measure the total temperature and pressure, respectively, in the settling chambers of the 11-inch hypersonic tunnel and the 22-inch helium tunnel. A pressure transducer was used to measure the pressure of the nitrogen in the arc chamber of the Langley hotshot tunnel. This pressure, together with the initial density, was used to calculate the total temperature in the arc chamber. Pressure transducers were used to measure the total pressure behind the normal shock in all three test facilities. An ionization gage was used to measure the base pressure in the 11-inch hypersonic tunnel. Base pressure was not measured for the tests conducted in either the 22-inch helium tunnel or the Langley hotshot tunnel.

ACCURACY OF DATA

The maximum uncertainties in the force and moment coefficients as determined from static calibration of the strain-gage balances are listed in the following table:

Parameter	11-inch hypersonic tunnel	Hotshot tunnel	22-inch helium tunnel
C_N . . .	±0.015	±0.014	±0.005
C_A . . .	±0.015		±0.002
C_m . . .	±0.011	±0.004	±0.001

The error in setting the angle of attack was less than $\pm 0.1^\circ$ in all three test facilities.

MODELS

The model used in the investigation was a 10° semiapex angle cone with varying nose bluntness. The bluntness ratio, defined as the ratio of nose radius to base radius, ranged from zero for the pointed cone to 0.763 for the bluntest configuration. A photograph of the models is presented in figure 2. The models tested in the 11-inch tunnel were constructed of stainless steel. Those tested in the hotshot tunnel and the 22-inch helium tunnel were constructed of magnesium. A detailed drawing of the models is presented in figure 3.

Geometrical equations in terms of bluntness ratio, cone angle, and base radius are presented in the appendix. These equations are useful for studying the effects of increasing bluntness ratio and cone angle on the correlation, as well as in the application of the correlation technique.

THEORY

Newtonian Impact Theory

Newtonian impact theory is compared with the experimental force- and moment-coefficient data obtained in the present investigation. The tables and equations presented in reference 13 were used to calculate the force and moment coefficients. The basic geometric parameter used in reference 13 was h/a, where in the present analysis $h = r_n \cos \phi$ and $a = r_b$. In terms of the bluntness ratio this parameter becomes

$$\frac{h}{a} = \psi \cos \phi \tag{1}$$

The equations presented in reference 13 for spherically blunted cones can be written in terms of the bluntness ratios as follows:

$$C_N = \left(1 - \psi^2 \cos^2\phi\right) C_{N,c} + \psi^2 C_{N,s} \tag{2}$$

$$C_A = \left(1 - \psi^2 \cos^2\phi\right) C_{A,c} + \psi^2 C_{A,s} \tag{3}$$

$$C_{m,b} = \frac{\cot \phi}{6}\left[\left(1 - 2\tan^2\phi\right)\left(1 - \psi^3\cos^3\phi\right) - 3\left(1 - \psi \cos \phi\right)\left(\psi^2\cos^2\phi\right)\right] C_{N,c} + \frac{\psi^2}{2}\left[\left(1 - \psi \cos \phi\right)\cot \phi - \psi \sin \phi\right] C_{N,s} \tag{4}$$

The moment reference length is $2r_b$ and reference area A_b for equations (2), (3), and (4). The moment center is located at the juncture of the X-axis and the base of the cone.

The Newtonian expression for the pressure coefficient may be written as

$$C_p = 2 \cos^2\eta \tag{5}$$

where η is the angle between the unit normal to the surface and wind vectors. Experience has indicated that the pressure distribution on a spheric body at hypersonic speeds is somewhat lower than that predicted by equation (5). However, the pressure distribution does approximately follow the cosine-square law and immediately suggests replacing the coefficient 2 with the stagnation-pressure coefficient behind the normal shock, $C_{p,max}$. The stagnation-pressure coefficient behind the normal shock is given by

$$C_{p,max} = \frac{2}{\gamma M_\infty^2}\left\{\left[\frac{(\gamma + 1)M_\infty^2}{2}\right]^{\frac{\gamma}{\gamma-1}}\left[\frac{\gamma + 1}{2\gamma M_\infty^2 - (\gamma - 1)}\right]^{\frac{\gamma}{\gamma-1}} - 1\right\} \tag{6}$$

By using equation (6) the so-called modified Newtonian expression for the pressure coefficient is obtained

$$C_p = C_{p,max} \cos^2\eta \tag{7}$$

Equation (7) is suggested in reference 19 and is compared in reference 13 with the more exact solution of reference 20. Reference 21 suggests that equation (6) be replaced by

$$C_{p,max} = \frac{\gamma + 3}{\gamma + 1}\left[1 - \frac{2}{M_\infty^2(\gamma + 3)}\right] \tag{8}$$

the limit of which, as $M_\infty \to \infty$, becomes $(\gamma + 3)/(\gamma + 1)$.

In reference 22 it is shown that equation (5) predicts the pressure distribution on slender cones but tends to overpredict the pressure distribution as the cone semiapex angle increased. For cones with large semiapex angles, equation (7) has been found to yield satisfactory results. In the present investigation two methods were used. The first assumed that equation (5) was valid for the entire body and the second assumed that equations (7) and (8) were valid. These will be referred to as pure Newtonian theory and modified Newtonian theory, respectively.

Force-Coefficient and Moment-Coefficient Correlations

A method for correlating normal-force and pitching-moment coefficients as a function of body geometry and angle of attack for spherically blunted cones is presented in reference 1. In the following development this method is presented, and the effects of increasing bluntness ratio, cone angle, and angle of attack on the correlation are studied. The parameters used in the correlations are developed from body geometry and Newtonian impact theory.

Normal-Force Coefficient

Case I, $\alpha \geq \phi$.- Newtonian impact theory predicts that the pressure coefficient along the most windward ray of a cone will be constant and proportional to the square of the sine of the angle between the tangent to the ray and the free-stream-velocity vector, that is

$$C_{p,w} = 2 \sin^2(\alpha + \phi) \tag{9}$$

Now for slender cones, where $(\alpha + \phi)$ is small, equation (9) may be written as

$$C_{p,w} \propto (\alpha + \phi)^2 \tag{10}$$

Next, assuming a circumferential pressure-coefficient distribution of the form (see fig. 4)

$$C_p = C_{p,w} \cos^2\theta \tag{11}$$

the normal-force coefficient may be written as

$$C_N = \frac{1}{A_b} \int_s C_p \, dA_p \tag{12}$$

Integration of equation (12) yields

$$C_N \propto C_{p,w}\left(\frac{A_p}{A_b}\right) \tag{13}$$

The ratio of planform area to base area may be written as (see eq. (A12))

$$\frac{A_p}{A_b} \approx \frac{A_{\bar{p}}}{A_b} \propto \frac{(1 - \psi^2)}{\phi} \tag{14}$$

where $A_b = \pi r_b^2$. Next, substituting equations (10) and (14) into equation (13)

$$C_N \propto \left[\phi + \alpha\left(2 + \frac{\alpha}{\phi}\right)\right](1 - \psi^2) \tag{15}$$

which for $\alpha \gg \phi$ reduces to

$$C_N \propto \alpha\left(2 + \frac{\alpha}{\phi}\right)(1 - \psi^2) \tag{16}$$

Case II, $\alpha < \phi$.- The normal-force coefficient can be written as (see ref. 12)

$$C_N \propto \cos^2\phi \sin 2\alpha \tag{17}$$

which for slender cones reduces to

$$C_N \propto 2\alpha \tag{18}$$

The parameter $\alpha\left(2 + \frac{\alpha}{\phi}\right)(1 - \psi^2)$ expressed in equation (16) reduces to equation (18) for $\alpha \ll \phi$ which is in agreement with case II. This parameter will be used to correlate normal-force coefficients for data obtained in the present investigation as well as those presented in reference 23.

Pitching-Moment Coeffficient

The pitching-moment coefficient about the nose of a spherically blunted cone may be written as

$$C_{m,n} = \frac{1}{A_b d} \int_{L_1}^{L_2} C_{p,w}\left(x - L_1 + r_n\right) r \, dx \tag{19}$$

This expression can be integrated by using equations (13) and (14) together with the relations

$$r = x \tan \phi \approx x\phi$$

$$L_1 = r_n \cot \phi \approx \frac{r_n}{\phi}$$

$$L_2 = r_b \cot \phi \approx \frac{r_b}{\phi}$$

to yield

$$C_{m,n} \propto C_N \left[\psi\left(\frac{1 - \phi}{\phi}\right) - \frac{2}{3\phi}\left(\frac{1 - \psi^3}{1 - \psi^2}\right) \right] \tag{20}$$

The parameter $\psi\left(\frac{1 - \phi}{\phi}\right) - \frac{2}{3\phi}\left(\frac{1 - \psi^3}{1 - \psi^2}\right)$ will be used to correlate the pitching-moment coefficients for the data obtained in the present investigation as well as those presented in reference 23.

The correlation parameters for normal-force and pitching-moment coefficients for spherically blunted cones have been derived by using Newtonian impact theory and simplified geometric relationships together with two main assumptions. These assumptions were: (1) that the cones were slender and (2) that the contribution of the spherical nose to the forces and moments was negligible.

RESULTS AND DISCUSSION

Force and Moment Data

Force-coefficient and pitching-moment-coefficient data obtained in the 11-inch hypersonic tunnel are presented in figure 5. Pitching-moment coefficient about the base $C_{m,b}$ and normal-force coefficient C_N were found to decrease with increasing bluntness ratio for a given angle of attack. Axial-force coefficient C_A for model IV was nearly independent of angle of attack for $\alpha \leqq 35^\circ$ and decreased for $\alpha > 35^\circ$. The drag coefficient C_D increased with increasing bluntness ratio for $\alpha \leqq 33^\circ$ and decreased with increasing bluntness ratio for $\alpha > 33^\circ$.

Maximum lift coefficient $C_{L,max}$ and maximum lift-drag ratio $(L/D)_{max}$ ranged from 0.89 to 0.31 and 1.49 to 0.32 for models I and IV, respectively. The angle of attack for maximum lift-drag ratio ranged from approximately 10° for model I to 33° for model IV.

Comparison of Experimental and Theoretical Results

Comparisons of the experimental data obtained in the 11-inch hypersonic tunnel with Newtonian impact theory are presented in figures 6 and 7. Two methods for applying impact theory were used:

Pure Newtonian theory which assumes that the pressure-coefficient distribution is given by equation (5) and modified Newtonian theory which assumes that equations (7) and (8) are valid.

The normal-force coefficients C_N were predicted very well by pure Newtonian theory for models I and II (figs. 6(a) and (b)); however, the agreement between theory and experimental data for models III and IV was best for modified Newtonian theory. (See figs. 6(c) and (d).) This result was to be

expected since, as previously pointed out, pure Newtonian theory overpredicts the pressure distribution on a spherical surface whereas the agreement is improved considerably by using modified Newtonian theory. Both methods underestimated the axial-force coefficient C_A for models I, II, and III whereas the agreement was very good for model IV over most of the angle-of-attack range. This trend is primarily due to a decrease in the viscous-force contribution in the axial direction with increasing angle of attack and the decrease of viscous effects, in general, with increasing bluntness ratio. The disagreement between the predicted axial-force coefficients and experimental values can be attributed to the viscous contribution to axial force. In reference 24 the T' method was used to estimate the viscous contribution to the axial-force coefficient for a 10° semiapex angle cone. (See also ref. 25.) These values were added to the inviscid axial-force coefficient obtained from Newtonian impact theory. The sum of the inviscid and viscous axial-force coefficients was found to be in very good agreement with experimental data. The pitching-moment coefficient about the base $C_{m,b}$ for all models was predicted well over the entire angle-of-attack range by pure Newtonian theory. The actual magnitudes of the coefficients were predicted within the accuracy of the data for models I and II (figs. 6(a) and 6(b)). The agreement between Newtonian theory and experimental lift-drag ratio improved as bluntness increased. (See fig. 7(a).) Newtonian theory overpredicted the maximum lift-drag ratio of model I by approximately 50 percent. The disagreement between experimental $(L/D)_{max}$ and theory decreased as bluntness increased. (See fig. 7(b).) Newtonian theory underpredicted the angle of attack for $(L/D)_{max}$ by approximately 2° for all four models. (See fig. 7(c).)

From these results it is apparent that Newtonian impact theory accurately predicts the trends of the aerodynamic characteristics for the sharp and spherically blunted cones through the 45° angle-of-attack range. In many instances the actual magnitudes of the force and moment coefficients were quite accurately predicted. The agreement between theory and experimental axial-force-coefficient data was found to improve with increasing bluntness ratio. This trend is a result of the decrease in the viscous contribution to axial force in comparison with the pressure force contribution.

Air-Helium Comparison

The data obtained in the 22-inch helium tunnel are compared with the 11-inch hypersonic tunnel air data and the hotshot tunnel nitrogen data in figures 8 and 9. Normal-force and pitching-moment coefficients are found to be nearly duplicated in all three facilities. Axial-force coefficients for models I, II, and III were somewhat lower in helium than in air. This difference decreased with increasing angle of attack and bluntness ratio. The axial-force coefficients for model IV were nearly duplicated in helium. The maximum lift-drag ratio of model I was approximately 15 percent higher in helium than in air. (See fig. 9.) This difference was caused by the lower viscous contribution to drag in helium than in air. The lift-drag ratio for the spherically blunted cones was nearly duplicated. The angle of attack for maximum lift-drag ratio was approximately the same as in air for all four models. The differences in

axial-force coefficients and consequently in lift-drag ratio can be attributed to Reynolds number differences of the tests rather than to specific-heat ratios. (See ref. 24.)

From an analysis of these data it is apparent that helium facilities can be adequately used to obtain aerodynamic data for spherically blunted cones within the range of test variables and model geometry considered. This is in agreement with the data presented in references 6 to 10. However, one should not extend the results of the present analysis or those of the previously mentioned references to include more complicated configurations with extensive interference flow fields and/or large separated flow regions. There is reason to suspect that the results obtained in helium may be unacceptable for such configurations. (See ref. 5.)

Normal-Force-Coefficient Correlation

The normal-force-coefficient data obtained in the present investigation together with data for other cone angles from reference 23 are presented as a function of the correlation parameter $\alpha\left(2 + \frac{\alpha}{\phi}\right)\left(1 - \psi^2\right)$ in figure 10. Normal-force-coefficient data were found to correlate reasonably well for $\phi = 10^\circ$ and $\psi \leqq 0.509$; however, the data for $\psi = 0.763$ were somewhat higher than the trend established by the lower bluntness ratios. The degree of correlation is seen to be relatively independent of bluntness ratio for $\psi \leqq 0.509$, but very dependent on cone semiapex angle ϕ. That is, as ϕ increases the region over which the data correlate decreases. (See fig. 10(a).) A theoretical study of the correlation parameter using Newtonian impact theory is presented in figure 11. This study clearly predicts the trends established in figure 10 by the data from the present investigation for a constant cone angle with varying bluntness ratio and the data from reference 23 for a nearly constant bluntness ratio with varying cone angle.

One of the main assumptions made in the derivation of the correlation parameter was that the contribution of the spherical nose to C_N was negligible. This assumption is studied in figure 12 for a range of bluntness ratios, cone angles, and angles of attack. For $\phi = 10^\circ$ and $\psi = 0.509$, the percentage of C_N due to the spherical nose is approximately 14 percent for $\alpha = 10^\circ$ and 10 percent for $\alpha = 40^\circ$. (See fig. 12(a).) Thus for a given bluntness ratio and cone angle the percentage of C_N due to the spherical nose decreases with increasing angle of attack. For $\phi = 40^\circ$ and $\psi = 0.509$, the percentage of C_N due to the spherical nose is independent of angle of attack for $\alpha \leqq 40^\circ$ and has a value of approximately 8 percent. From this it is clear that the assumption is even more justified for increasing cone angle. For bluntness ratios above 0.5 the percentage of C_N due to the spherical nose increases rapidly, for example, for $\phi = 10^\circ$ and $\psi = 0.763$ the percentage of C_N due to the spherical nose is approximately 40 percent for $\alpha = 10^\circ$. (See fig. 12(a).)

In order to obtain a compact and useful expression for the normal-force-coefficient-correlation parameter $\alpha\left(2 + \frac{\alpha}{\phi}\right)\left(1 - \psi^2\right)$, it was necessary to assume

that the quantity $(\alpha + \phi)$ was small. (See eq. (10).) It is of interest to note that the analysis of the experimental data from the present investigation together with those from reference 23 indicate that the degree of correlation was not restricted to cases where $(\alpha + \phi)$ was small, but only to cases where $\sin \phi \approx \phi$.

In the preceding discussion it was shown that the percentage of C_N due to the spherical nose for bluntness ratios less than 0.509 is no more than 10 to 15 percent of the total C_N for the spherically blunted 10° semiapex angle cone. Furthermore, it was shown that the correlation was restricted to cases where $\sin \phi \approx \phi$. With this in mind, a third-order polynomial was fitted to the data for the sharp cone, model I, and the resulting equation may be written as

$$C_N = 0.0285 + 0.6097\xi - 0.1061\xi^2 + 0.0095\xi^3 \tag{21}$$

where

$$\xi = \alpha\left(2 + \frac{\alpha}{\phi}\right)(1 - \psi^2)$$

Equation (21) should yield reasonably accurate estimations of the normal-force coefficients for conical bodies where $\psi \leq 0.5$ and $\sin \phi \approx \phi$.

Pitching-Moment-Coefficient Correlation

The pitching-moment-coefficient data obtained in the present investigation together with data for other cone angles from reference 23 are presented as a function of the correlation parameter, $C_N\left(\frac{\bar{x}}{r_b}\right)_{approx}$, in figure 13(a). The parameter $\left(\frac{\bar{x}}{r_b}\right)_{approx}$ defines the approximate location of the centroid of the planform area neglecting the spherical nose. From equation (20) one finds that (see eq. (A11)),

$$\left(\frac{\bar{x}}{r_b}\right)_{approx} = \frac{2}{3\phi}\left(\frac{1 - \psi^3}{1 - \psi^2}\right) - \psi\left(\frac{1 - \phi}{\phi}\right)$$

A considerable amount of scatter in the experimental data was found to exist when the data were correlated against the approximate centroid location of the planform area as proposed in reference 1. (See fig. 13(a).) However, most of this scatter was removed by using the exact location of the centroid of the planform area including the planform area of the spherical nose. (See fig. 13(b).) This parameter can be easily found by using the equations given in the appendix. (See eqs. (A7) and (A8).) The parameter $\left(\frac{\bar{x}}{r_b}\right)_{exact}$ is the distance between the nose of the body and the centroid of its planform area normalized by the base radius r_b and can be expressed as

$$\left(\frac{\bar{x}}{r_b}\right)_{exact} = \frac{1}{r_b}\frac{\sum_{i=1}^{4} A_i\bar{x}_i}{\sum_{i=1}^{4} A_i} + \psi(1 - \csc \phi) \qquad (22)$$

All the 10° semiapex angle cone data are found to lie nearly on the line defined by

$$C_{m,n} = -\frac{C_N}{2}\left(\frac{\bar{x}}{r_b}\right)_{exact} \qquad (23)$$

Equation (23) is nearly identical in form to the correlation curve presented in reference 1; however, a nonlinear relationship exists between $\left(\frac{\bar{x}}{r_b}\right)_{approx}$ and $\left(\frac{\bar{x}}{r_b}\right)_{exact}$. The degree of correlation is found to be relatively independent of increasing bluntness ratio for $\phi = 10^\circ$ but very much dependent on increasing cone angle. For cone angles greater than 10°, equation (23) tends to underpredict the actual value of $C_{m,n}$ with the degree of inaccuracy increasing as ϕ increases. A theoretical study of the correlation parameter $\left(\frac{\bar{x}}{r_b}\right)_{exact}$ using Newtonian impact theory is presented in figure 14. This study clearly predicts the trends established in figure 13 by the data from the present investigation for a constant cone angle with varying bluntness ratio and the data from reference 23 for a nearly constant bluntness ratio with varying cone angle.

From the preceding discussion it is apparent that $C_{m,n}$ can be correlated as a function of body geometry and angle of attack for slender cones having small to moderate bluntness ratios. The degree of correlation is greatly improved by using equation (23) instead of the approximate location of the centroid of the planform area as proposed in reference 1.

Reynolds Number Effects

The Reynolds numbers studied during the investigation ranged from 0.75×10^5 to 6.12×10^5. As such, no conclusions can be made from these data as to the effect of lower Reynolds numbers on the values of C_N and $C_{m,n}$ obtained from equations (21) and (23), respectively. However, in reference 26, it was shown that for a slightly blunted 9° semiapex angle cone, reducing the free-stream Reynolds number per foot from 1.8×10^5 to 2.0×10^4 caused a substantial change in both C_N and C_m. The effect of Reynolds number on C_N and C_m would decrease with both increasing cone angle and bluntness ratio.

CONCLUSIONS

An experimental investigation in air, nitrogen, and helium of the aerodynamic characteristics of a 10° semiapex angle cone with several values of bluntness ratio at Mach numbers from 9.75 to 19.15 and Reynolds numbers from 0.75×10^5 to 6.12×10^5 for angles of attack from 0° to 45° has yielded the following conclusions:

1. Normal-force coefficients and pitching-moment coefficients in air can be correlated in terms of a parameter which includes bluntness ratio, cone angle, and angle of attack for slender cones having small to moderate bluntness ratios. The correlation would be expected to yield poor results for cone semiapex angles much larger than 10° and for bluntness ratios greater than 0.5.

2. Normal-force coefficients and pitching-moment coefficients obtained in air and nitrogen were nearly duplicated in helium. The differences in axial-force coefficients and consequently in lift-drag ratio, for the present investigation, can be attributed to the Reynolds number differences of the tests rather than to the differences in specific-heat ratios. Therefore, within the range of test variables and model geometry considered, helium facilities can be satisfactorily used to study the aerodynamic characteristics of blunted cones for the ideal-gas case.

3. Newtonian impact theory predicted the trends of the aerodynamic characteristics and in many instances predicted the actual magnitudes of the coefficients. Agreement between theory and experimental data was found to improve with increasing bluntness ratio.

Langley Research Center,
National Aeronautics and Space Administration,
Langley Station, Hampton, Va., July 22, 1964.

APPENDIX

GEOMETRICAL EQUATIONS FOR SHARP AND SPHERICALLY BLUNTED CONES

The geometrical equations for sharp and spherically blunted cones may be expressed in terms of bluntness ratio, cone angle, and base radius as (see fig. 4)

$$L = r_b\left[\psi(1 - \csc \phi) + \cot \phi\right] \tag{A1}$$

$$L_1 = r_b\psi \csc \phi \tag{A2}$$

$$L_2 = r_b \cot \phi \tag{A3}$$

$$x_m = r_b\psi \cos \phi \cot \phi \tag{A4}$$

$$r_m = r_b\psi \cos \phi \tag{A5}$$

$$r_n = r_b\psi \tag{A6}$$

The planform area may be found from

$$A_p = 2 \sum_{i=1}^{4} A_i \tag{A7}$$

where $i = 1, 2, 3, 4$ and

$$A_1 = \frac{r_b^2\psi^2}{2}\left(\frac{\pi}{2} - \phi\right) \tag{A7a}$$

$$A_2 = \frac{r_b^2\psi^2}{4} \sin 2\phi \tag{A7b}$$

$$A_3 = \frac{r_b^2}{2} \cot \phi(1 - \psi \cos \phi)^2 \tag{A7c}$$

$$A_4 = r_b^2 \psi \cot \phi \cos \phi (1 - \psi \sec \phi) \tag{A7d}$$

The centroid location of the planform area may be found from

$$\bar{x}_p = \frac{\sum_{i=1}^{4} A_i \bar{x}_i}{\sum_{i=1}^{4} A_i} \tag{A8}$$

where

$$\bar{x}_1 = \frac{r_b \psi \csc \phi}{3(\pi - 2\phi)} \left[3(\pi - 2\phi) - 2 \sin 2\phi \right] \tag{A8a}$$

$$\bar{x}_2 = \frac{r_b \psi}{3} \csc \phi (3 - \sin^2 \phi) \tag{A8b}$$

$$\bar{x}_3 = \frac{r_b}{3} \cot \phi (2 + \psi \cos \phi) \tag{A8c}$$

$$\bar{x}_4 = \frac{r_b}{2} \cot \phi (\psi \sec \phi + 1) \tag{A8d}$$

The planform area neglecting the spherical nose is

$$A_{\bar{p}} = 2(2A_2 + A_3 + A_4) \tag{A9}$$

The exact location of the planform area centroid neglecting the spherical nose is

$$\bar{x}_{\bar{p}} = \frac{2r_b \cot \phi (\psi^2 \cos^2 \phi + \psi \cos \phi + 1)}{3(1 + \psi \cos \phi)} + \psi (1 - \csc \phi) \tag{A10}$$

The approximate location of the planform area centroid may be written for slender cones as (see ref. 1)

$$\left(\bar{x}_{\bar{p}}\right)_{approx} = r_b\left[\frac{2}{3\phi}\left(\frac{1 - \psi^3}{1 - \psi^2}\right) - \psi\left(\frac{1 - \phi}{\phi}\right)\right] \tag{A11}$$

A very useful approximate expression for the planform area for slightly blunted cones can be developed as follows: Let

$$A_{\bar{p}} \approx r_b L_2 - r_n L_1$$

where for small ϕ

$$L_1 \approx \frac{r_n}{\phi}$$

$$L_2 \approx \frac{r_b}{\phi}$$

Thus one obtains

$$A_{\bar{p}} \approx r_b{}^2\left(\frac{1 - \psi^2}{\phi}\right) \tag{A12}$$

Equations (A1) to (A12) are useful in the application of the correlation technique to a specific body.

REFERENCES

1. Whitfield, Jack D.; and Wolny, W.: Hypersonic Static Stability of Blunt Slender Cones. AEDC-TDR-62-166 (Contract No. AF 40(600)-1000), Arnold Eng. Dev. Center, Aug. 1962.

2. Griffith, B. J.; and Wolny, W.: Sharp and Blunt Cone Force Tests at M_∞ = 17 and Various Reynolds Numbers. AEDC-TDR-62-67 (Contract No. AF 40(600)-800 S/A 24(61-73)), Arnold Eng. Dev. Center, Mar. 1962.

3. Love, Eugene S.; Henderson, Arthur, Jr.; and Bertram, Mitchel H.: Some Aspects of Air-Helium Simulation and Hypersonic Approximations. NASA TN D-49, 1959.

4. Mueller, James N.: Conversion of Inviscid Normal-Force Coefficients in Helium to Equivalent Coefficients in Air for Simple Shapes at Hypersonic Speeds. NACA TN 3807, 1956.

5. Seiff, Alvin: Recent Information on Hypersonic Flow Fields. Proceedings of the NASA-University Conference on the Science and Technology of Space Exploration, Vol. 2, NASA SP-11, 1962, pp. 269-282. (Also available as NASA SP-24.)

6. Ladson, Charles L.: Effects of Several Nose and Vertical-Fin Modifications on the Low-Angle-of-Attack Static Stability of a Winged Reentry Vehicle at Mach Numbers of 9.6 in Air and 17.8 in Helium. NASA TM X-608, 1961.

7. Ladson, Charles L.; and Blackstock, Thomas A. (With appendix by Donald L. Baradell and Thomas A. Blackstock): Air-Helium Simulation of the Aerodynamic Force Coefficients of Cones at Hypersonic Speeds. NASA TN D-1473, 1962.

8. Johnston, Patrick J.; and Snyder, Curtis D.: Static Longitudinal Stability and Performance of Several Ballistic Spacecraft Configurations in Helium at a Mach Number of 24.5. NASA TN D-1379, 1962.

9. Ladson, Charles L.: A Comparison of Aerodynamic Data Obtained in Air and Helium in the Langley 11-Inch Hypersonic Tunnel. NASA TM X-666, 1962.

10. Henderson, Arthur, Jr.: Recent Investigations of the Aerodynamic Characteristics of General and Specific Lifting and Nonlifting Configurations at Mach 24 in Helium, Including Air-Helium Simulation Studies. The High Temperature Aspects of Hypersonic Flow, Wilbur C. Nelson, ed., Pergamon Press, 1964, pp. 163-190.

11. Johnston, Patrick J.: Longitudinal Aerodynamic Characteristics of Several Fifth-Stage Scout Reentry Vehicles From Mach Number 0.60 to 24.4 Including Some Reynolds Number Effects on Stability at Hypersonic Speeds. NASA TN D-1638, 1963.

12. Grimminger, G.; Williams, E. P.; and Young, G. B. W.: Lift on Inclined Bodies of Revolution in Hypersonic Flow. Jour. Aero. Sci., vol. 17, no. 11, Nov. 1950, pp. 675-690.

13. Wells, William R.; and Armstrong, William O.: Tables of Aerodynamic Coefficients Obtained From Developed Newtonian Expressions for Complete and Partial Conic and Spheric Bodies at Combined Angles of Attack and Sideslip With Some Comparisons With Hypersonic Experimental Data. NASA TR R-127, 1962.

14. Rainey, Robert W.: Working Charts for Rapid Prediction of Force and Pressure Coefficients on Arbitrary Bodies of Revolution by Use of Newtonian Concepts. NASA TN D-176, 1959.

15. Smith, Fred M.; Harrison, Edwin F.; and Lawing, Pierce L.: Description and Initial Calibration of the Langley Hotshot Tunnel With Some Real-Gas Charts for Nitrogen. NASA TN D-2023, 1963.

16. McLellan, Charles H.; Williams, Thomas W.; and Bertram, Mitchel H.: Investigation of a Two-Step Nozzle in the Langley 11-Inch Hypersonic Tunnel. NACA TN 2171, 1950.

17. Stine, Howard A.; and Wanlass, Kent: Theoretical and Experimental Investigation of Aerodynamic Heating and Isothermal Heat-Transfer Parameters on a Hemispherical Nose With Laminar Boundary Layer at Supersonic Mach Numbers. NACA TN 3344, 1954.

18. Arrington, James P.; Joiner, Roy C., Jr.; and Henderson, Arthur, Jr.: Longitudinal Characteristics of Several Configurations at Hypersonic Mach Numbers in Conical and Contoured Nozzles. NASA TN D-2489, 1964.

19. Penland, Jim A.: Aerodynamic Characteristics of a Circular Cylinder at Mach Number 6.86 and Angles of Attack up to 90°. NACA TN 3861, 1957. (Supersedes NACA RM L54A14.)

20. Van Dyke, Milton D.; and Gordon, Helen D.: Supersonic Flow Past a Family of Blunt Axisymmetric Bodies. NASA TR R-1, 1959.

21. Lees, Lester: Hypersonic Flow. Fifth International Aeronautical Conference (Los Angeles, Calif., June 20-23, 1955), Inst. Aero. Sci., Inc., 1955, pp. 241-276.

22. Penland, Jim A.: Aerodynamic Force Characteristics of a Series of Lifting Cone and Cone-Cylinder Configurations at a Mach Number of 6.83 and Angles of Attack up to 130°. NASA TN D-840, 1961.

23. Armstrong, William O.: Hypersonic Aerodynamic Characteristics of Several Series of Lifting Bodies Applicable to Reentry Vehicle Design. NASA TM X-536, 1961.

24. Arrington, James P.; and Maddalon, Dal V.: Aerodynamic Characteristics of Several Lifting and Nonlifting Configurations at Hypersonic Speeds in Air and Helium. NASA TM X-918, 1964.

25. Monaghan, R. J.: An Approximate Solution of the Compressible Laminar Boundary Layer on a Flat Plate. R. & M. No. 2760, British A.R.C., 1956.

26. Wilkinson, David B.; and Harrington, Shelby A.: Hypersonic Force, Pressure, and Heat Transfer Investigations of Sharp and Blunt Slender Cones. AEDC-TDR-63-177 (Contract No. AF 40(600)-928), Arnold Eng. Dev. Center, Aug. 1963.

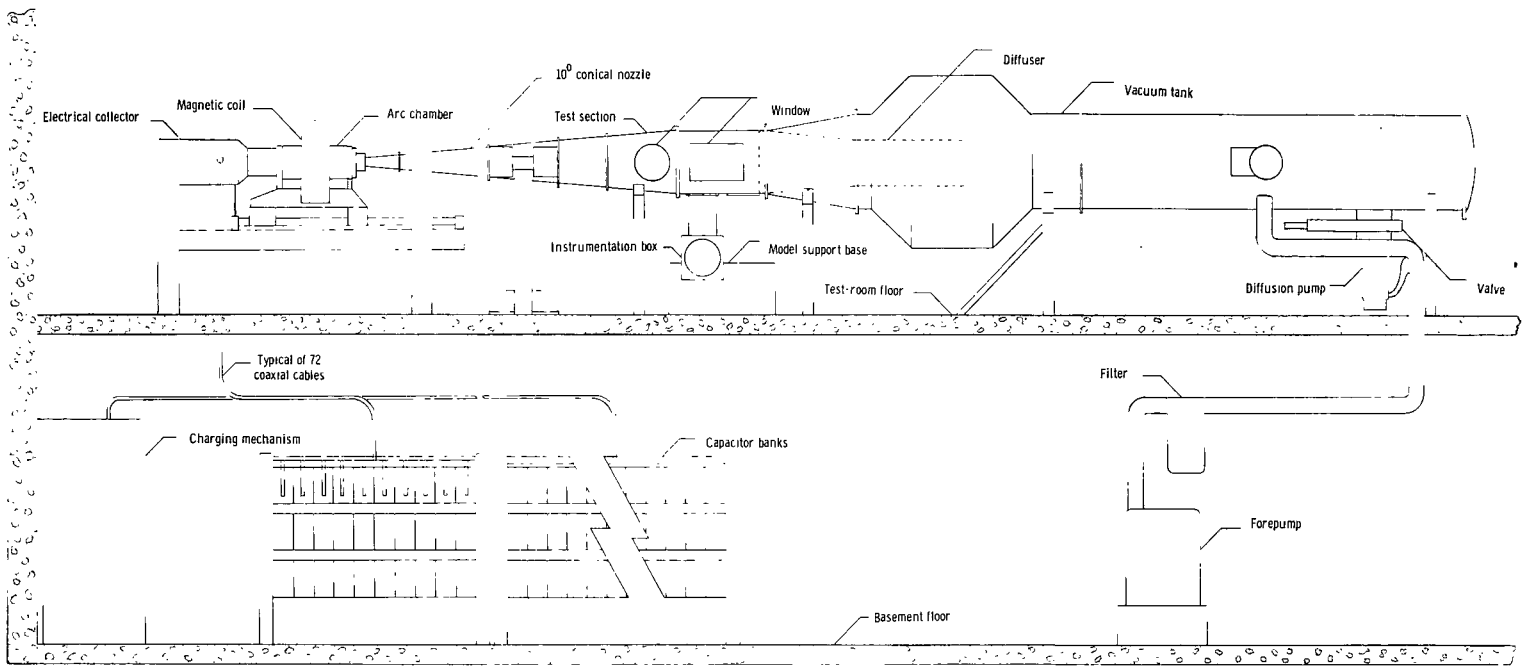

Figure 1.- Langley hotshot tunnel.

Figure 2.- Models.

L-63-9791

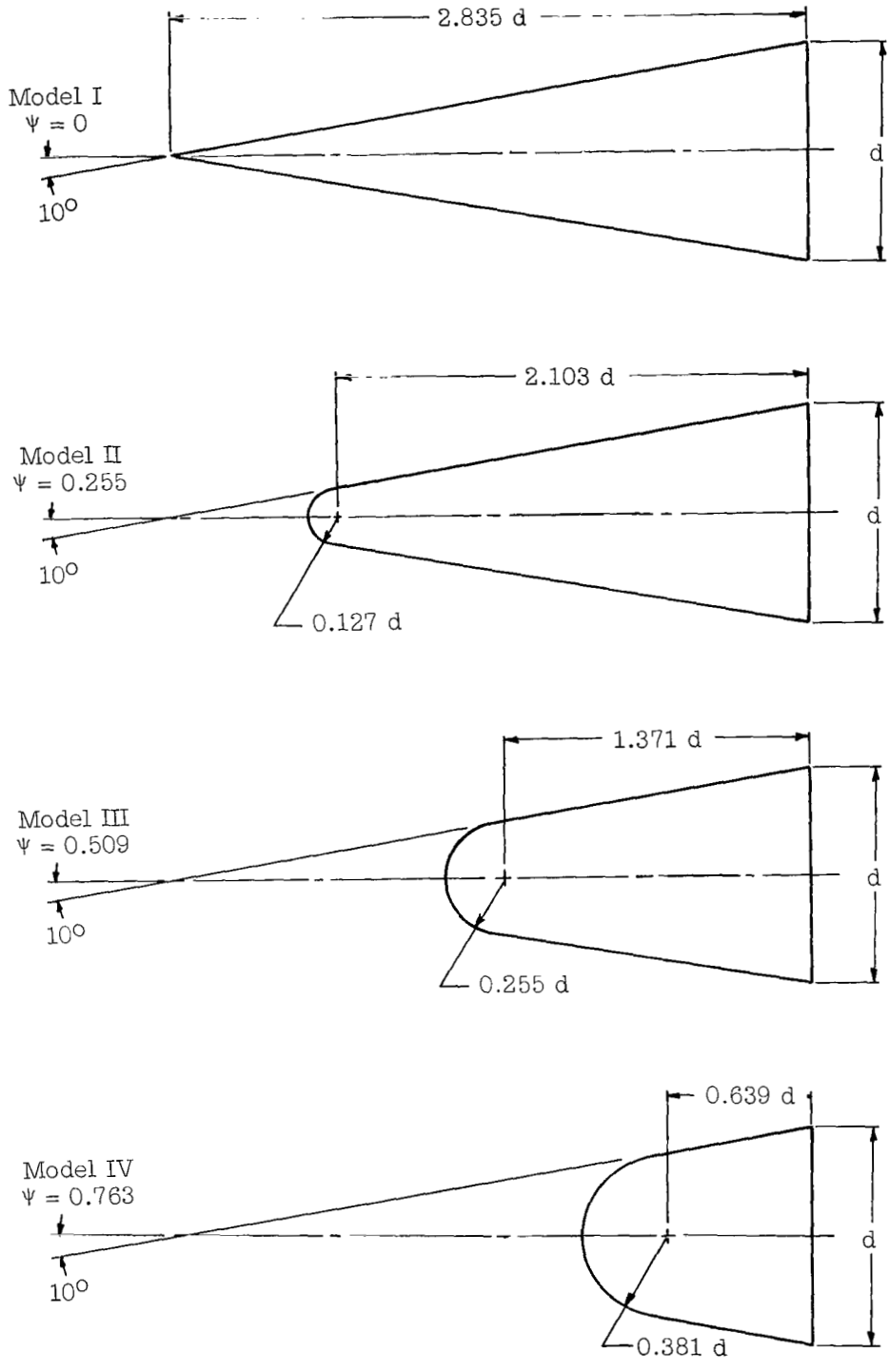

Figure 3.- Model drawings and dimensions. 11-inch hypersonic tunnel, d = 1.50 in.; 22-inch helium tunnel, d = 3.00 in.; hotshot tunnel, d = 3.00 in.

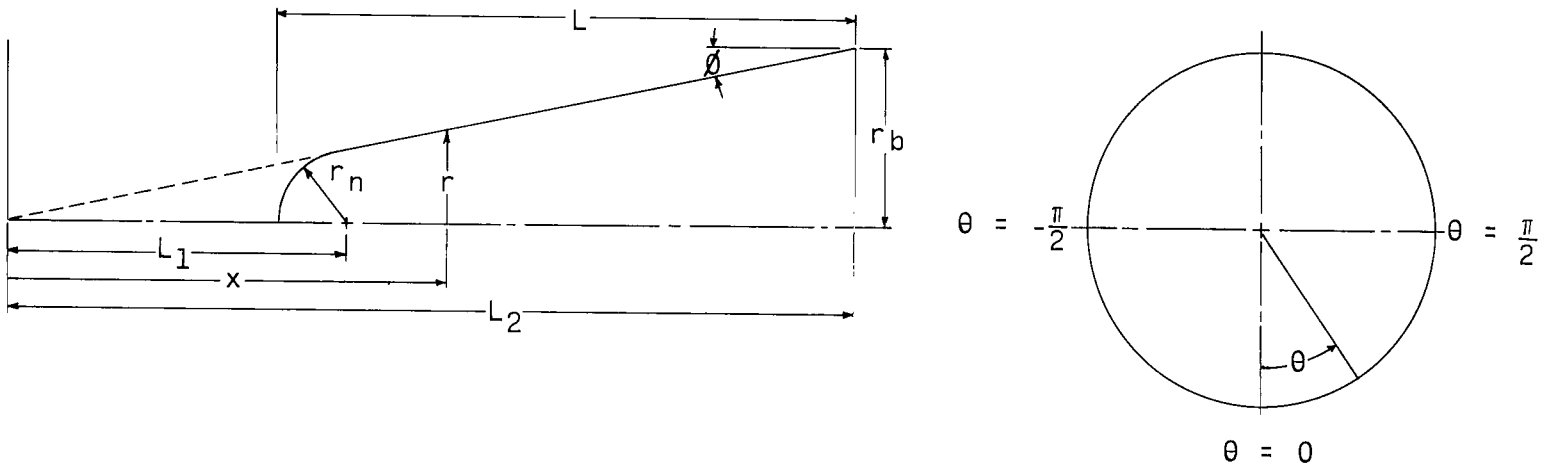

(a) Linear nomenclature.

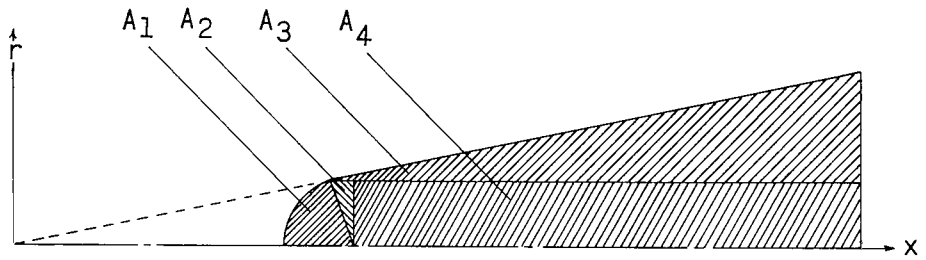

(b) Planform area nomenclature.

Figure 4.- Model geometry.

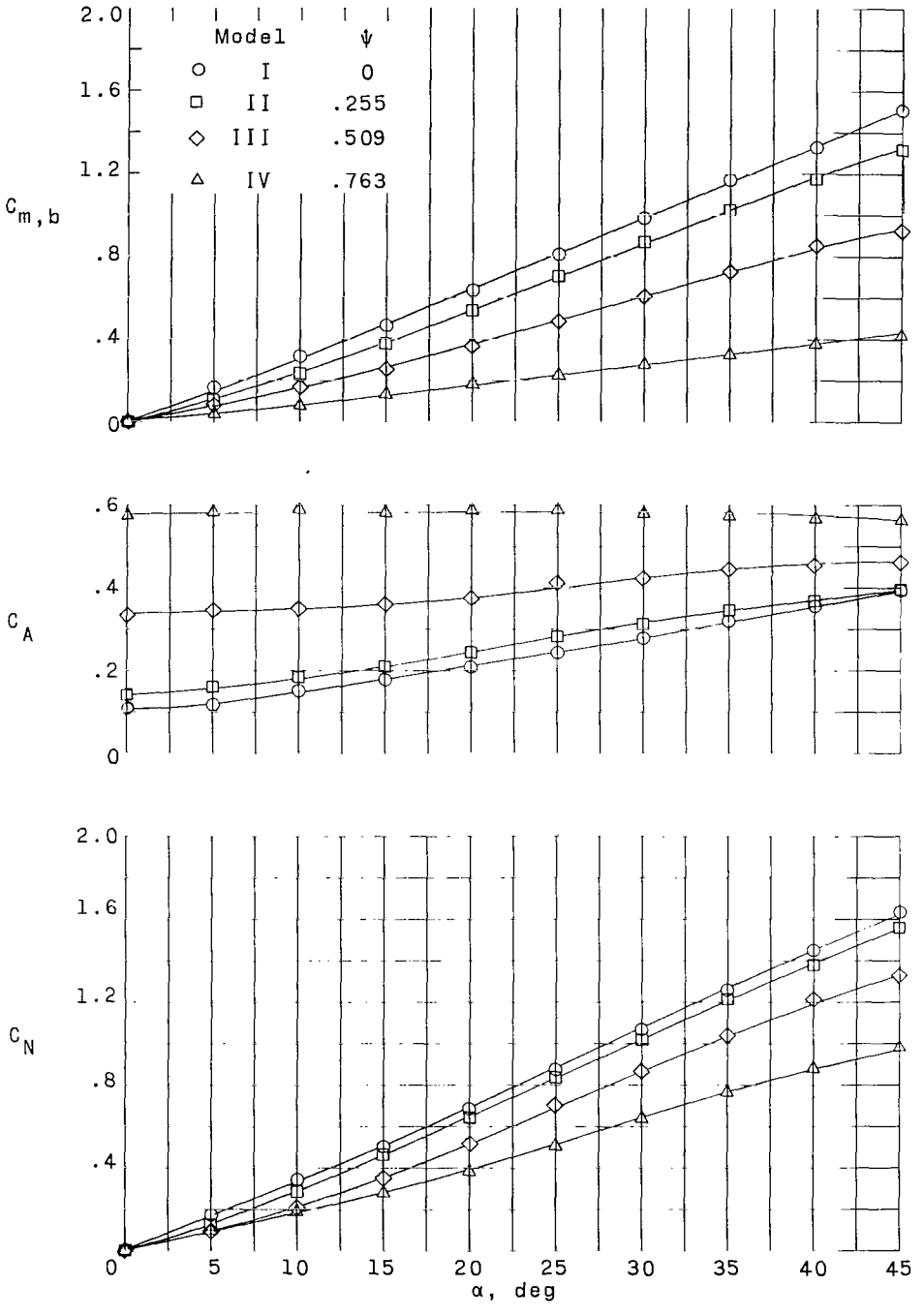

(a) Referred to the body-axis system.

Figure 5.- Effects of bluntness ratio on the longitudinal force characteristics of a 10° semiapex angle cone; $M_\infty = 9.75$; $R = 1.56 \times 10^5$; $\gamma = 7/5$.

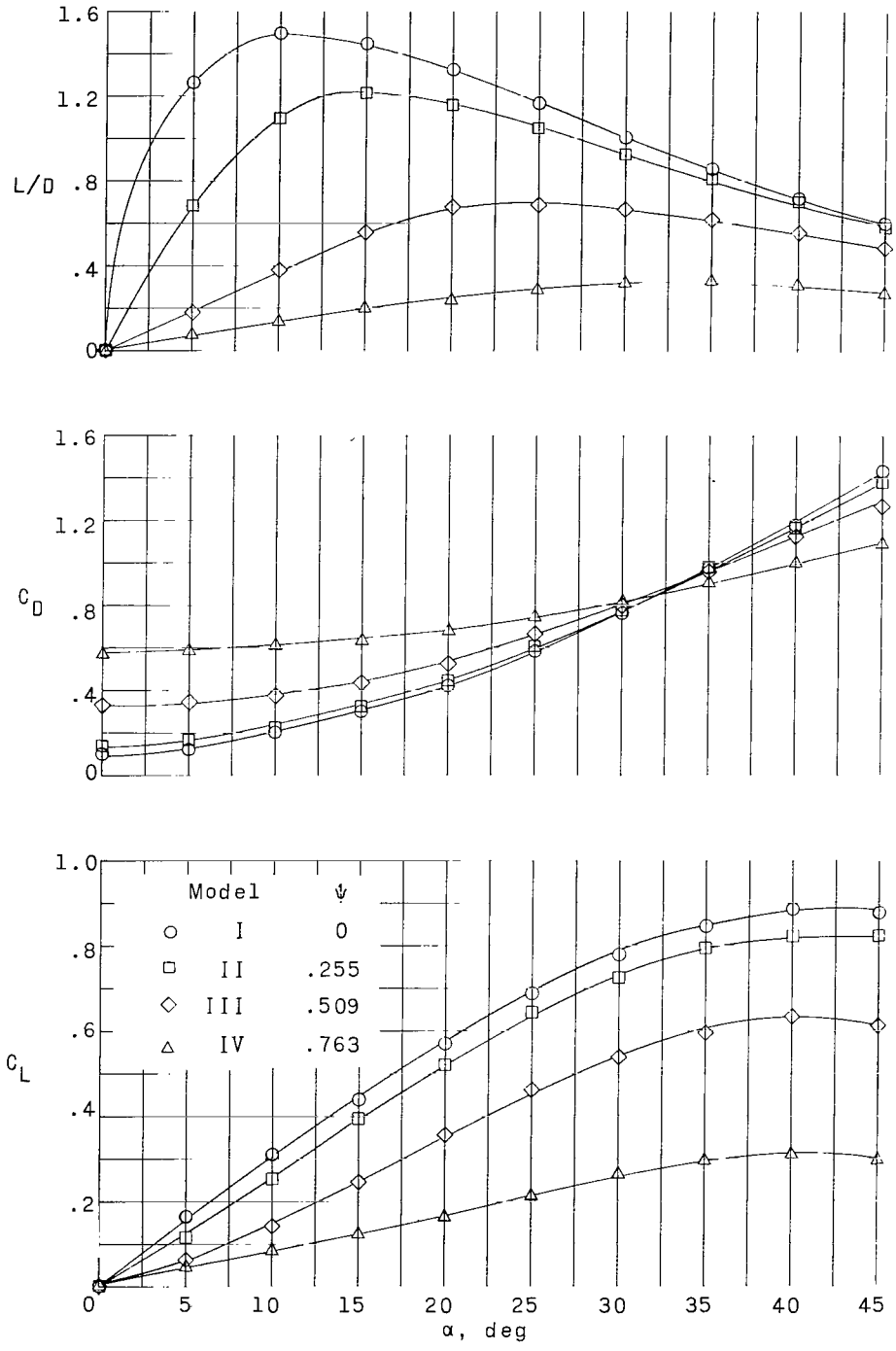

(b) Referred to the stability-axis system.

Figure 5.- Concluded.

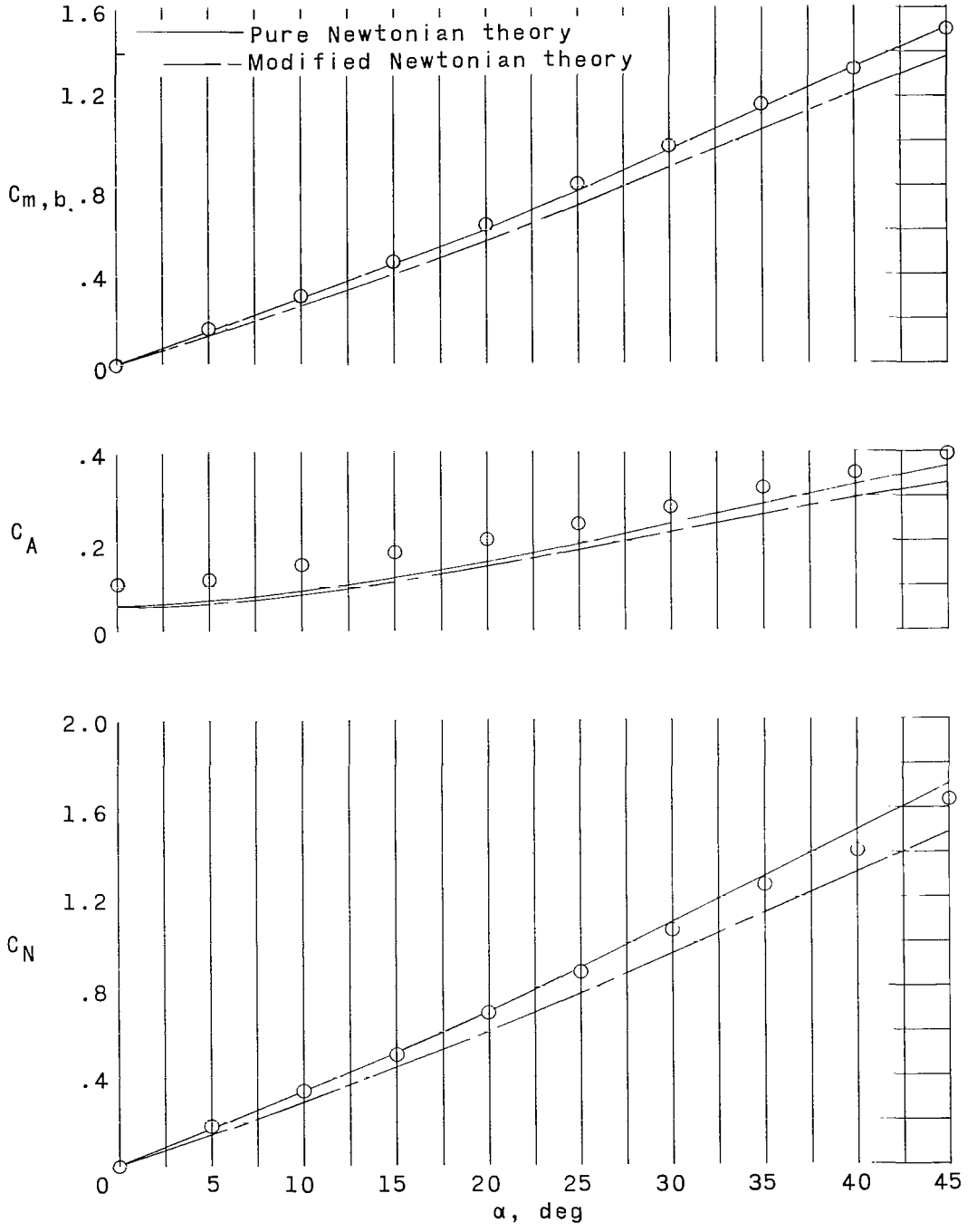

(a) Model I; $\psi = 0$.

Figure 6.- Comparison with theory of the longitudinal force characteristics for a 10° semiapex angle cone with various bluntness ratios; $M_{\infty} = 9.75$; $R = 1.56 \times 10^5$; $\gamma = 7/5$.

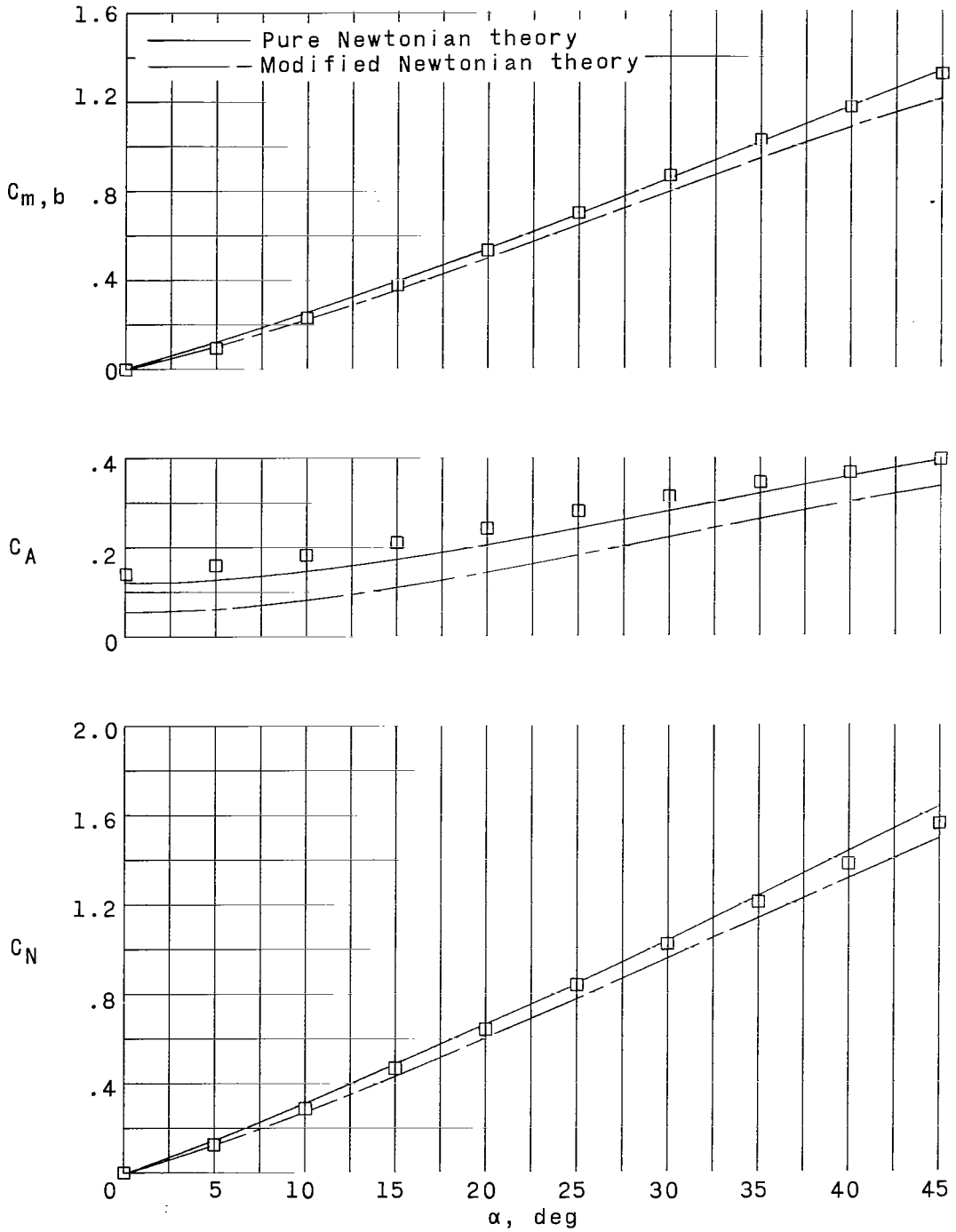

(b) Model II; ψ = 0.255.

Figure 6.- Continued.

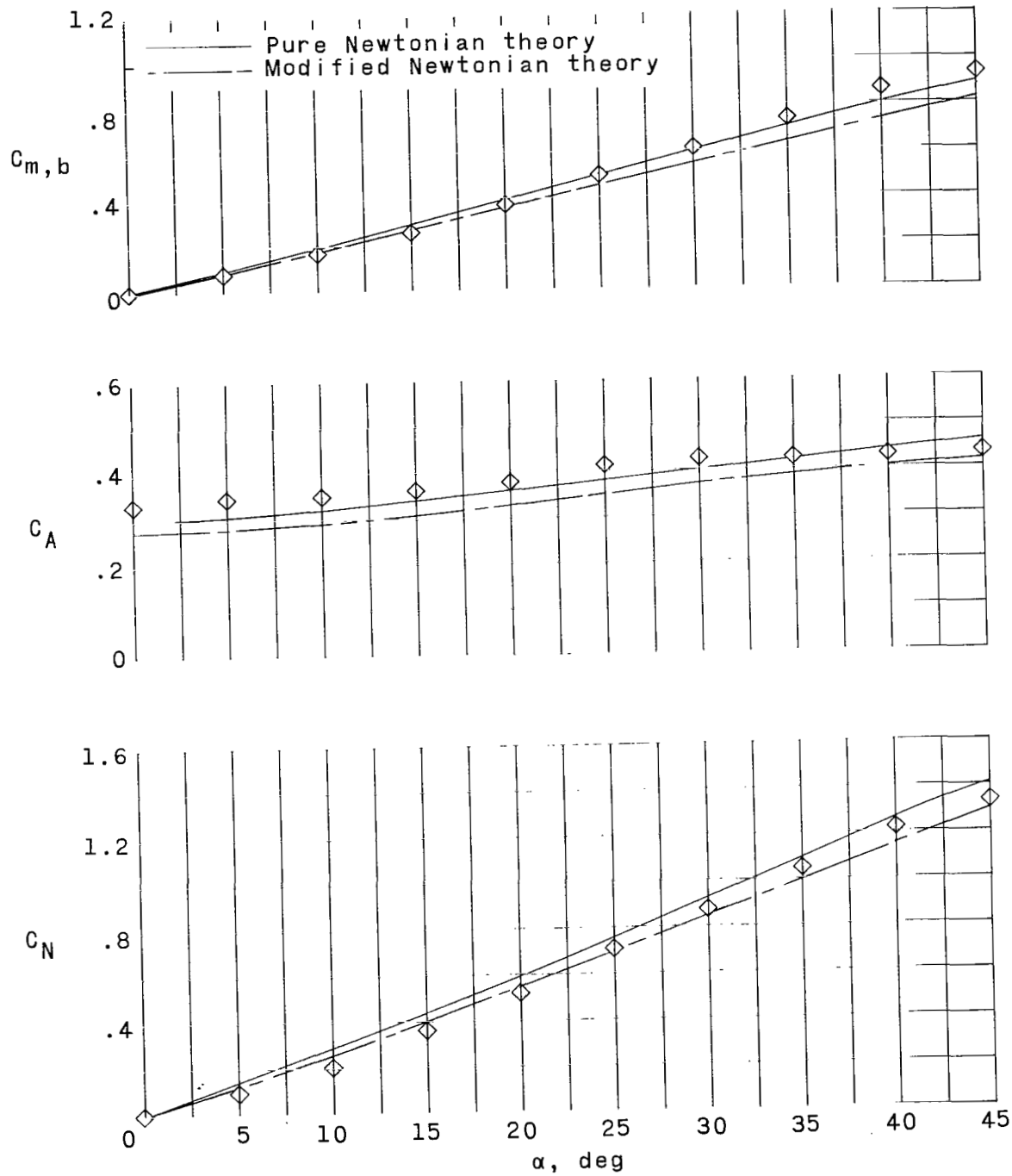

(c) Model III; $\psi = 0.509$.

Figure 6.- Continued.

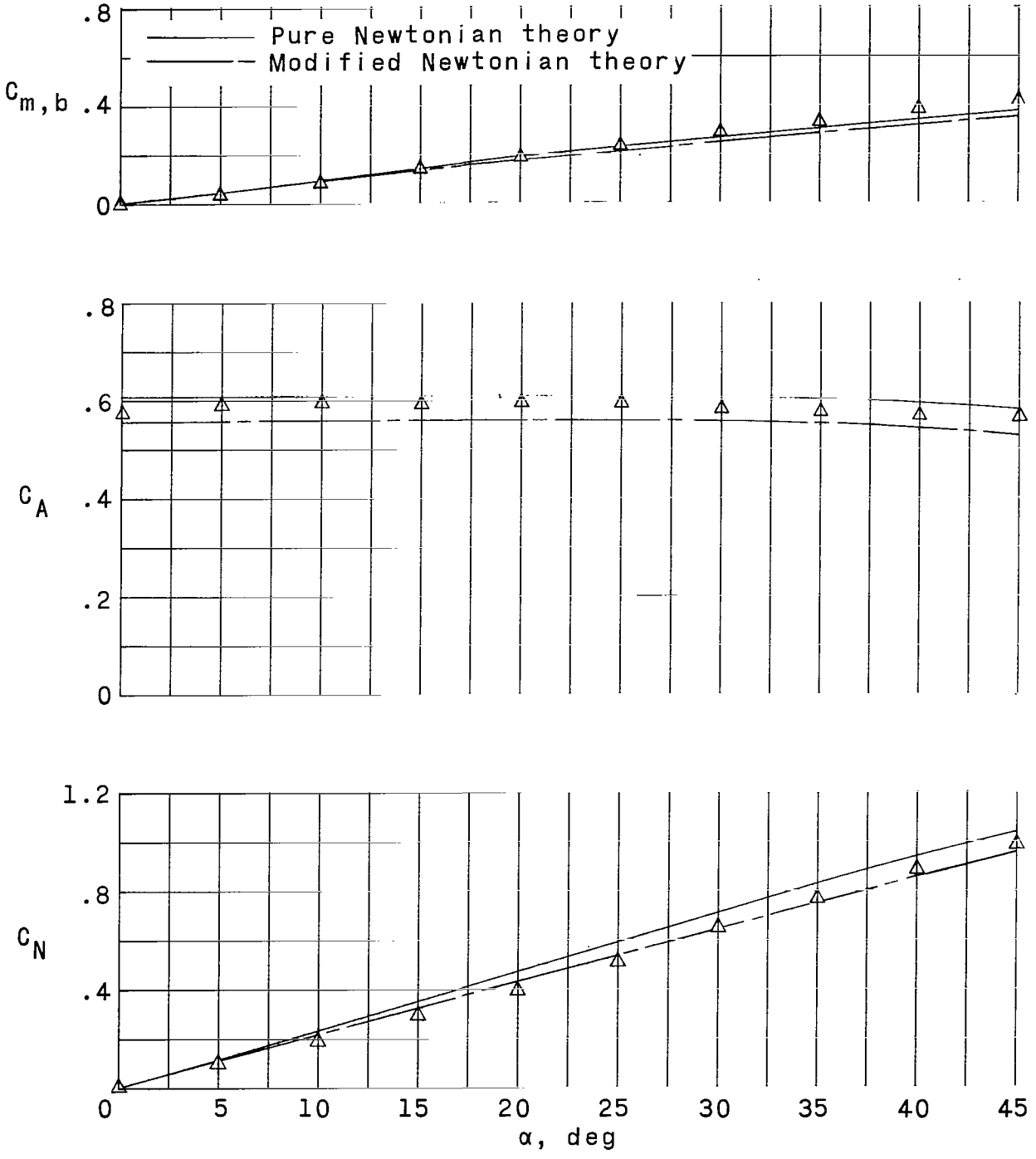

(d) Model IV; ψ = 0.763.

Figure 6.- Concluded.

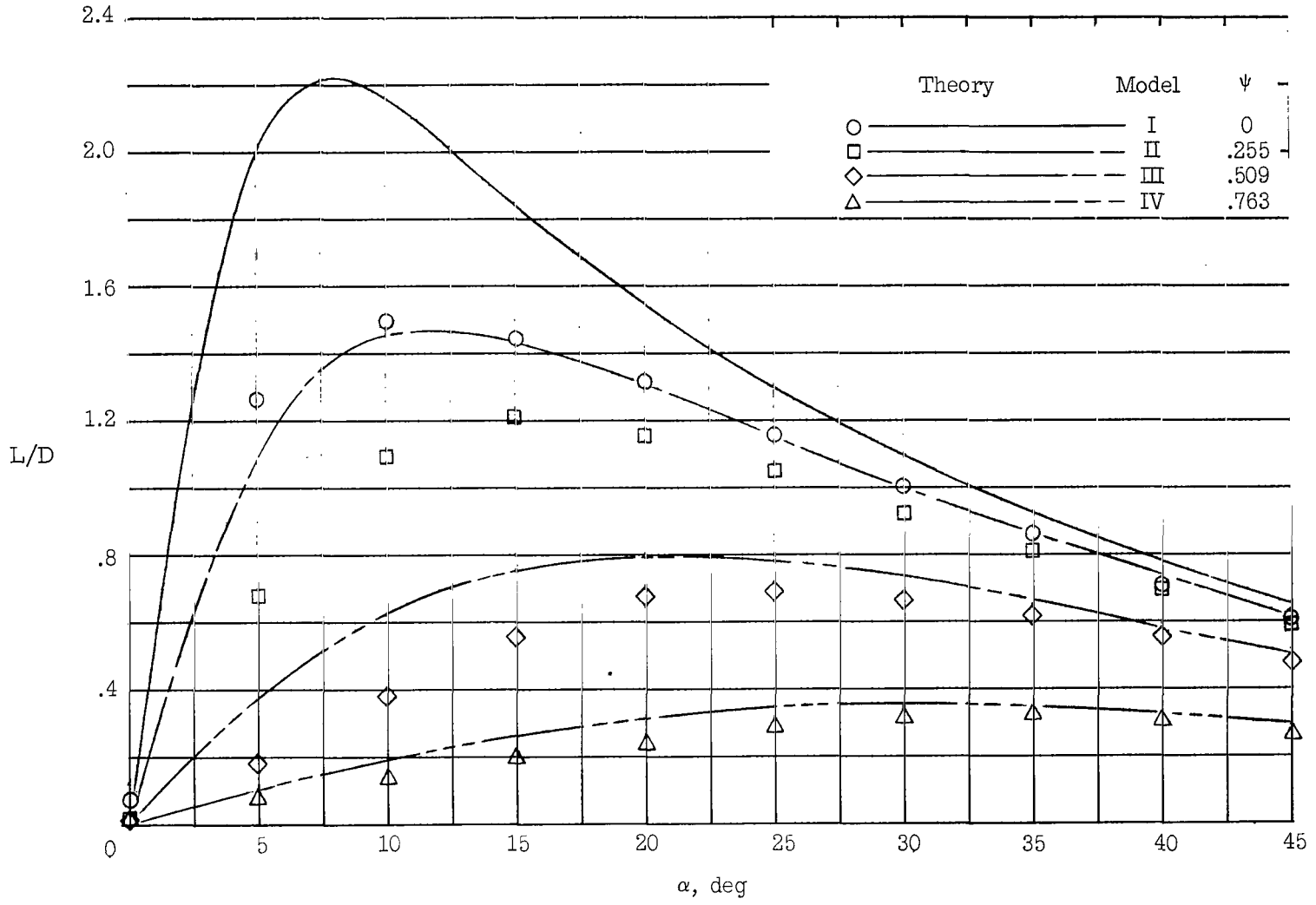

(a) Lift-drag ratio.

Figure 7.- Lift-drag-ratio study for a 10° semiapex angle cone with various bluntness ratios; $M_\infty = 9.75$; $R = 1.56 \times 10^5$; $\gamma = 7/5$.

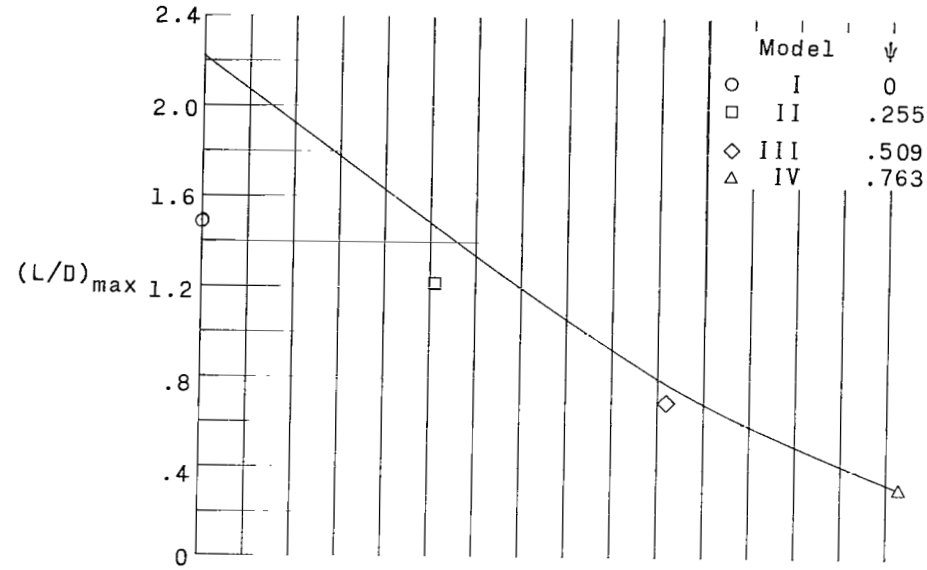

(b) Maximum lift-drag ratio.

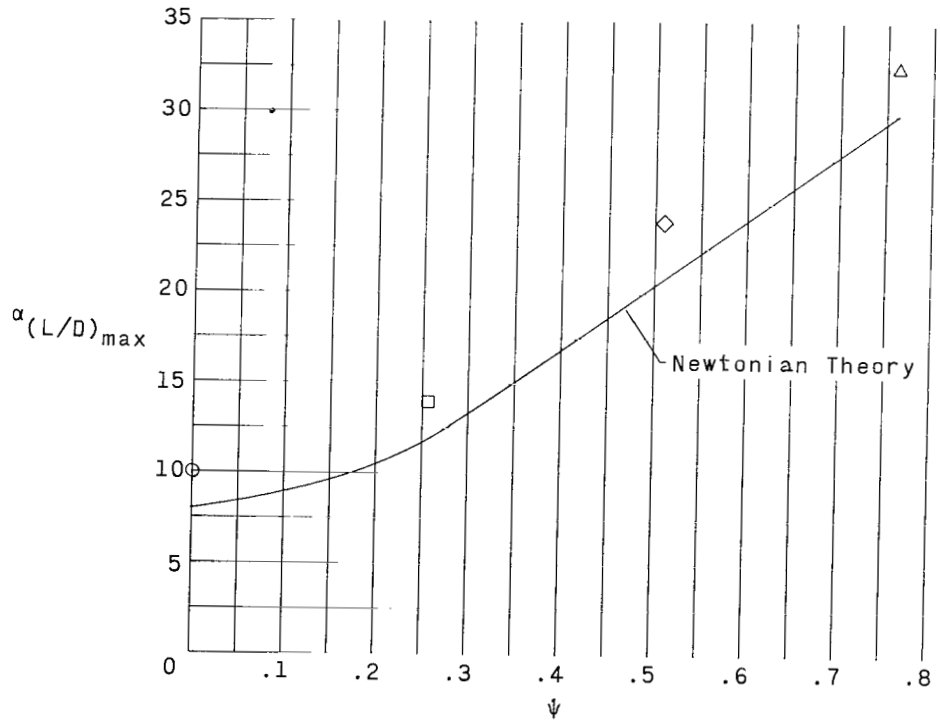

(c) Angle of attack for maximum lift-drag ratio.

Figure 7.- Concluded.

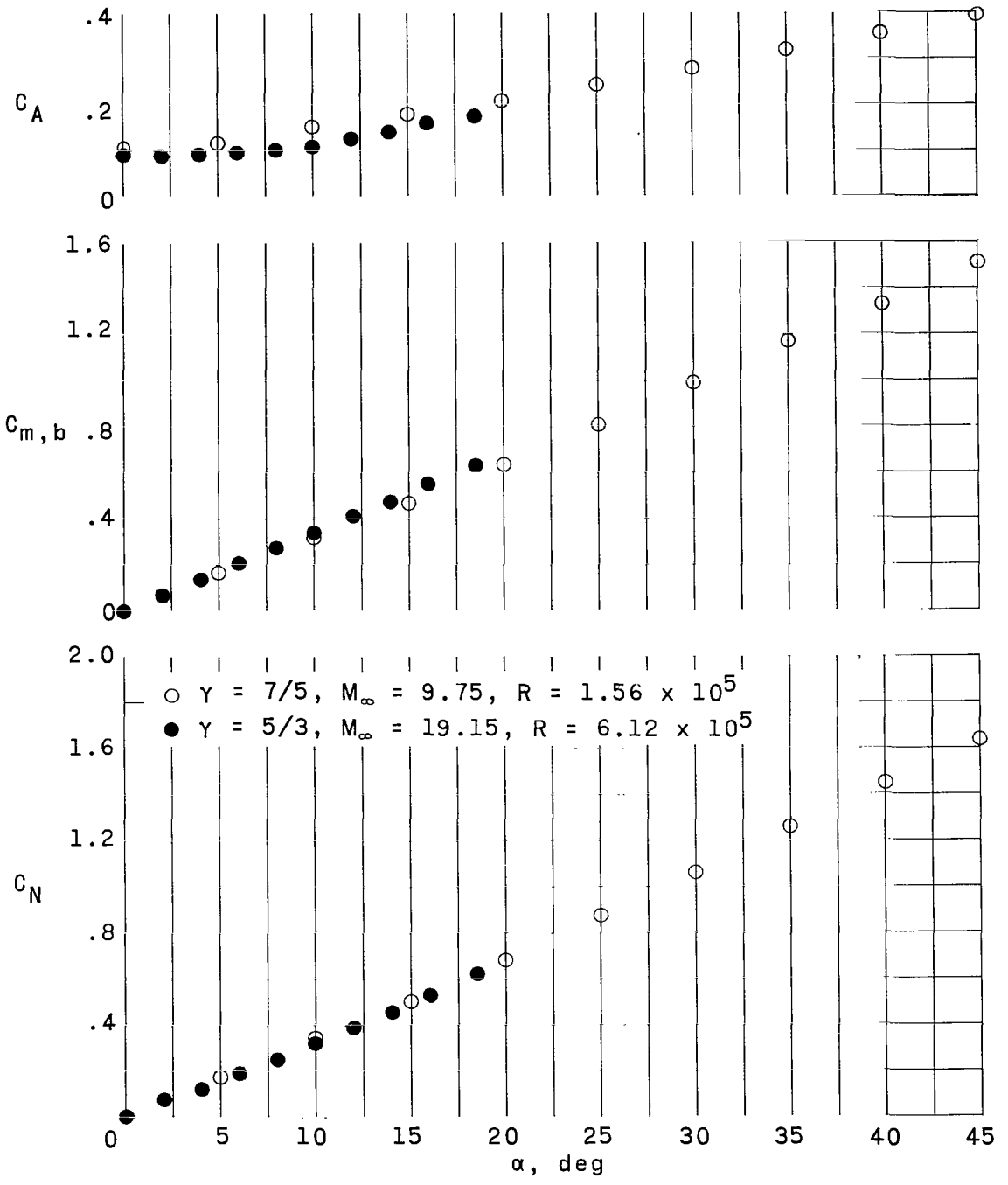

(a) Model I; $\psi = 0$.

Figure 8.- Comparison of longitudinal force characteristics of a 10° semiapex angle cone with various bluntness ratios in air, nitrogen, and helium.

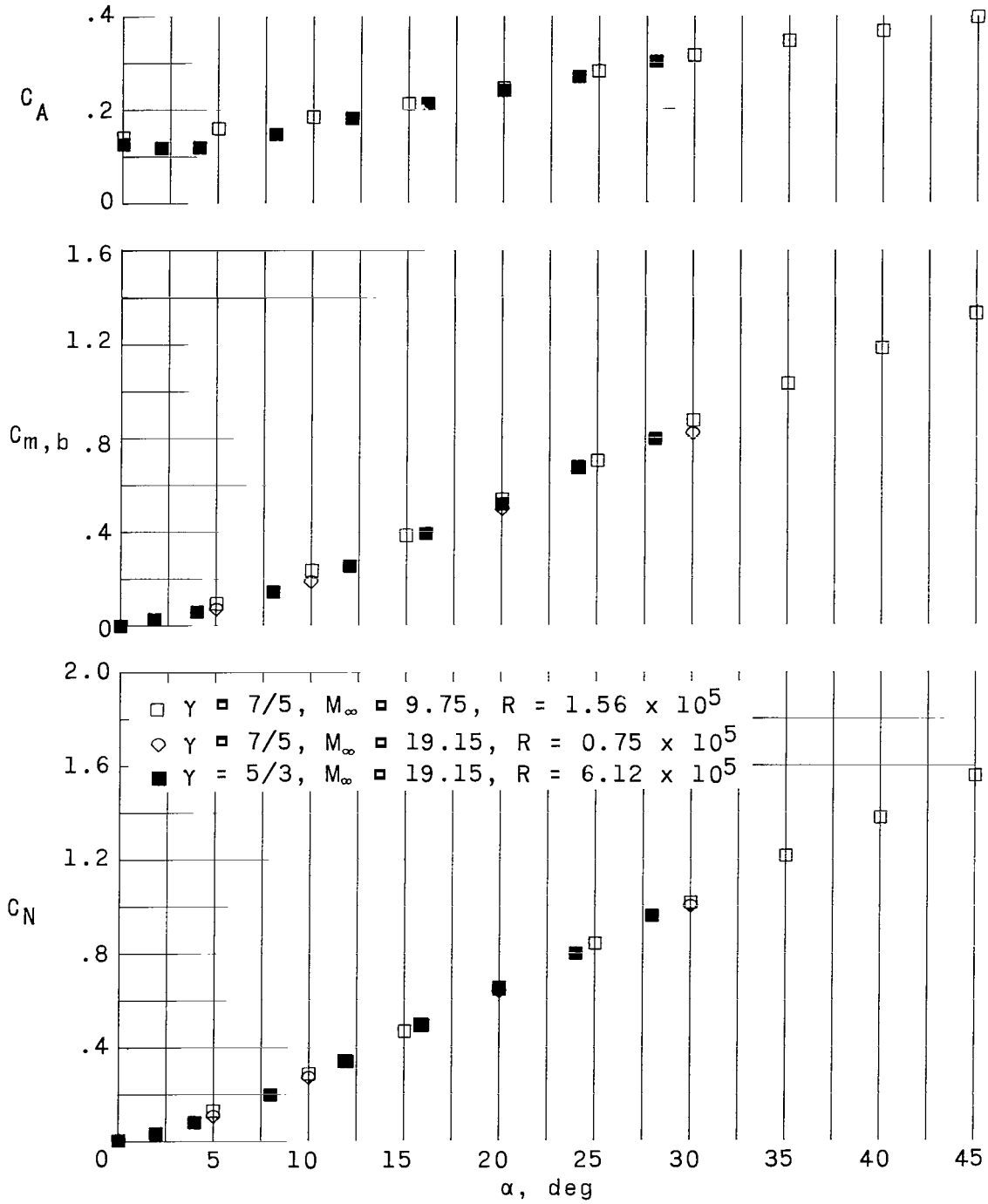

(b) Model II; ψ = 0.255.

Figure 8.- Continued.

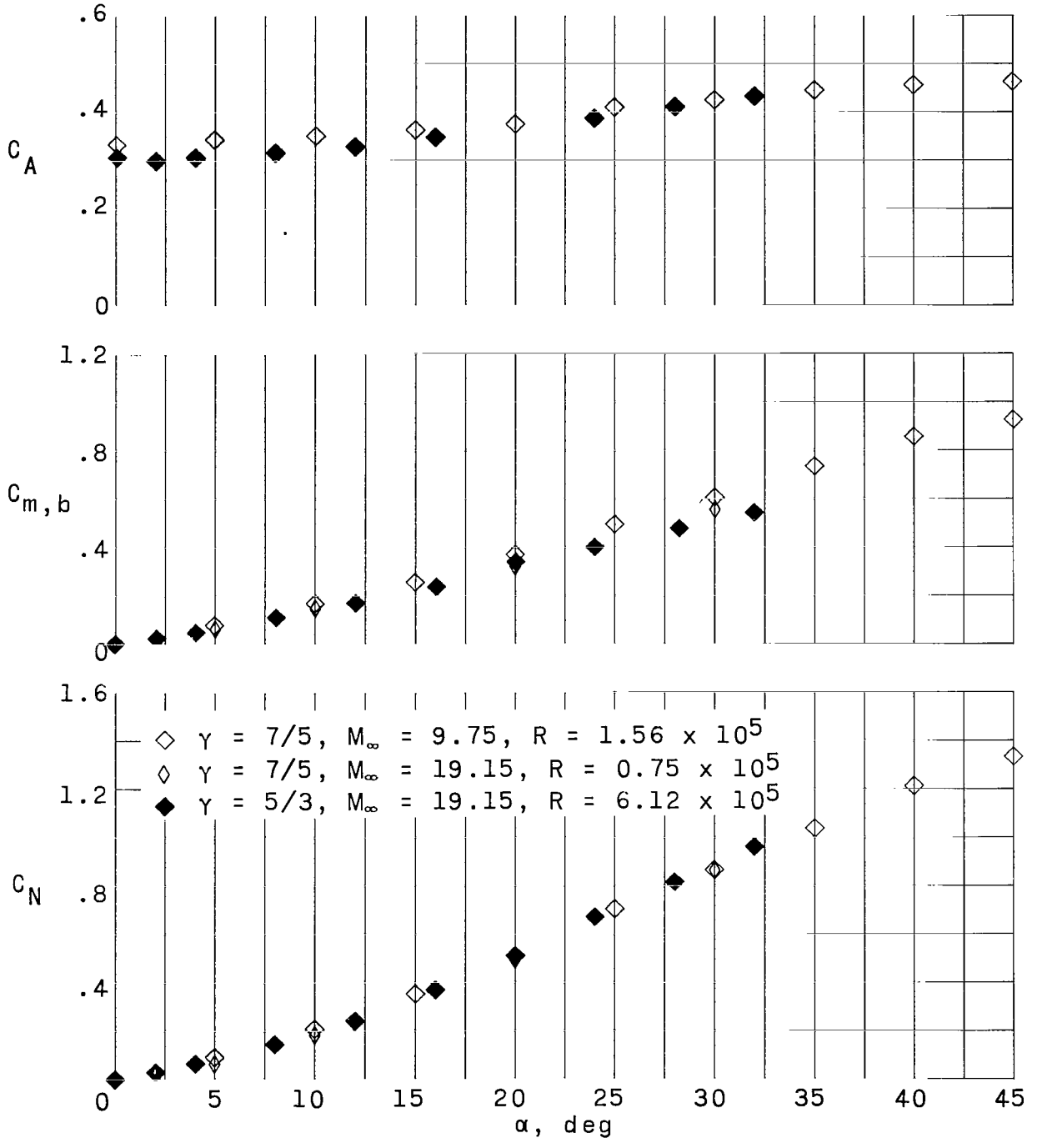

(c) Model III; ψ = 0.509.

Figure 8.- Continued.

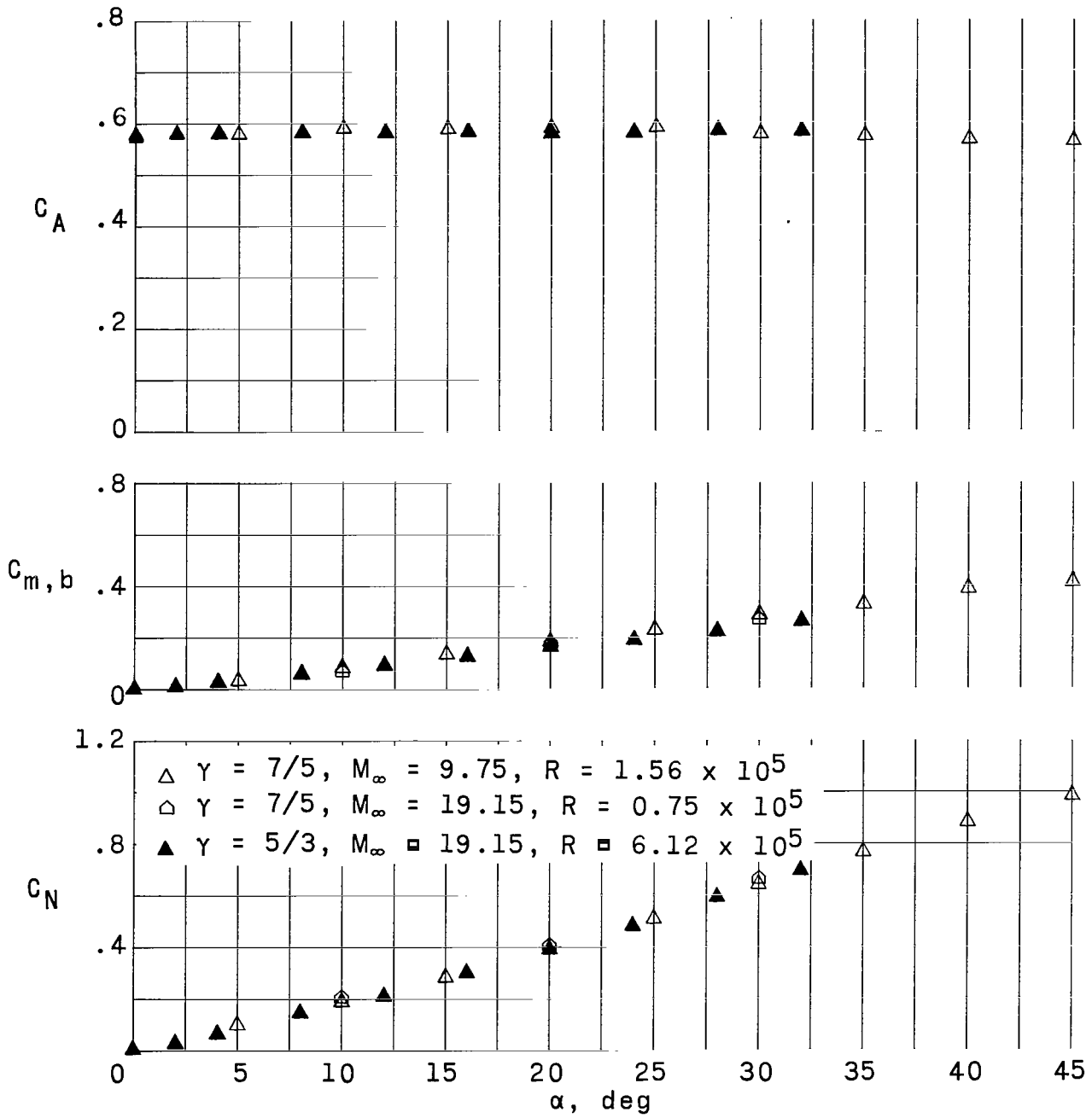

(d) Model IV; ψ = 0.763.

Figure 8.- Concluded.

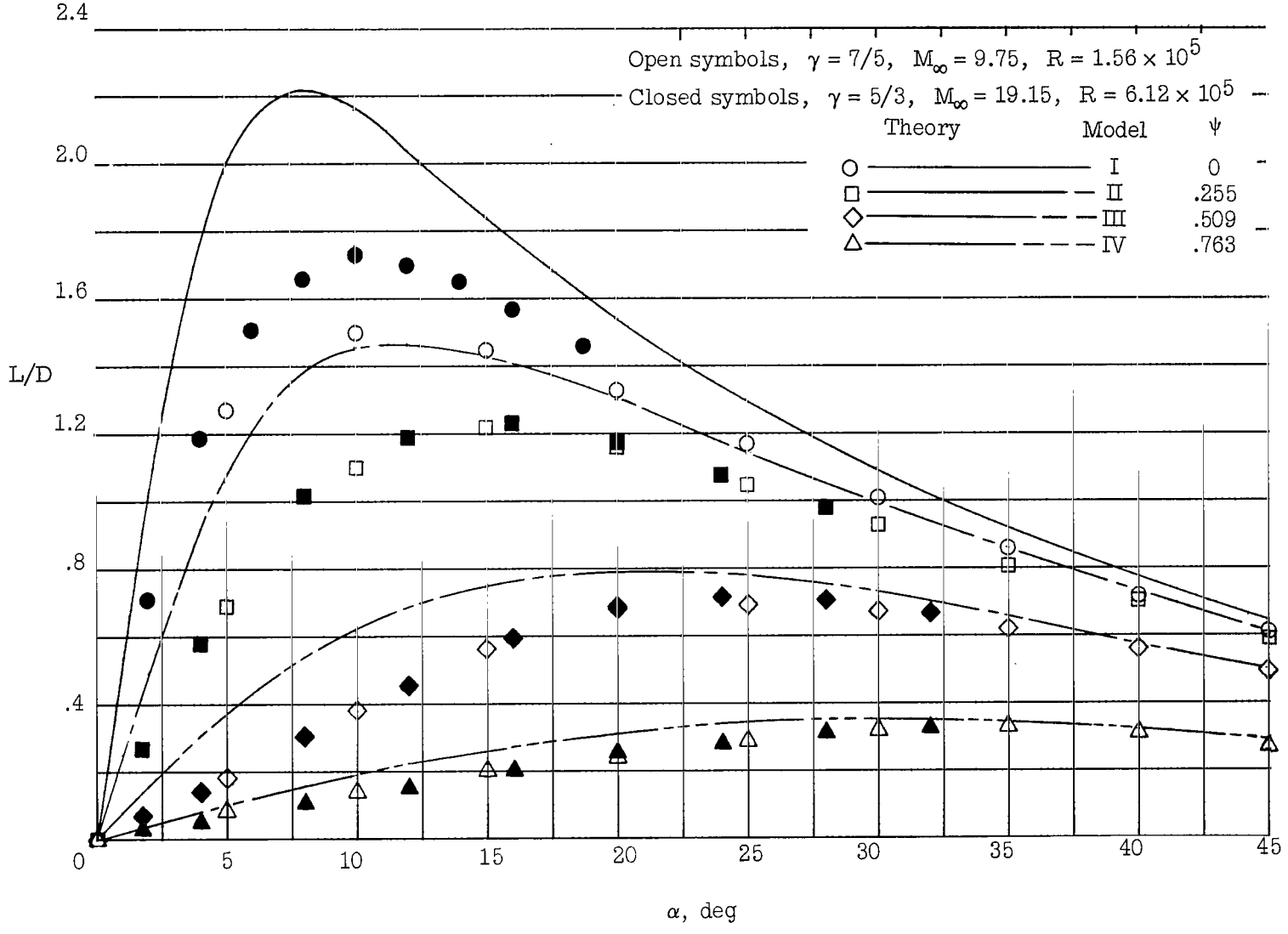

Figure 9.- Comparison of lift-drag ratio for a 10° semiapex angle cone with various bluntness ratios in air and helium.

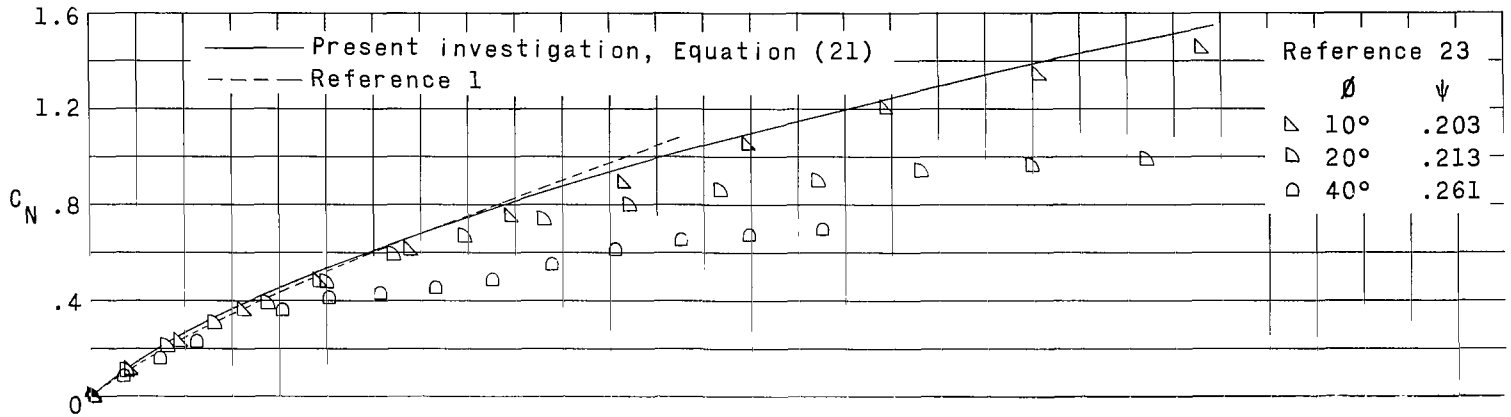

(a) Effect of cone angle; $\psi \approx 0.226$.

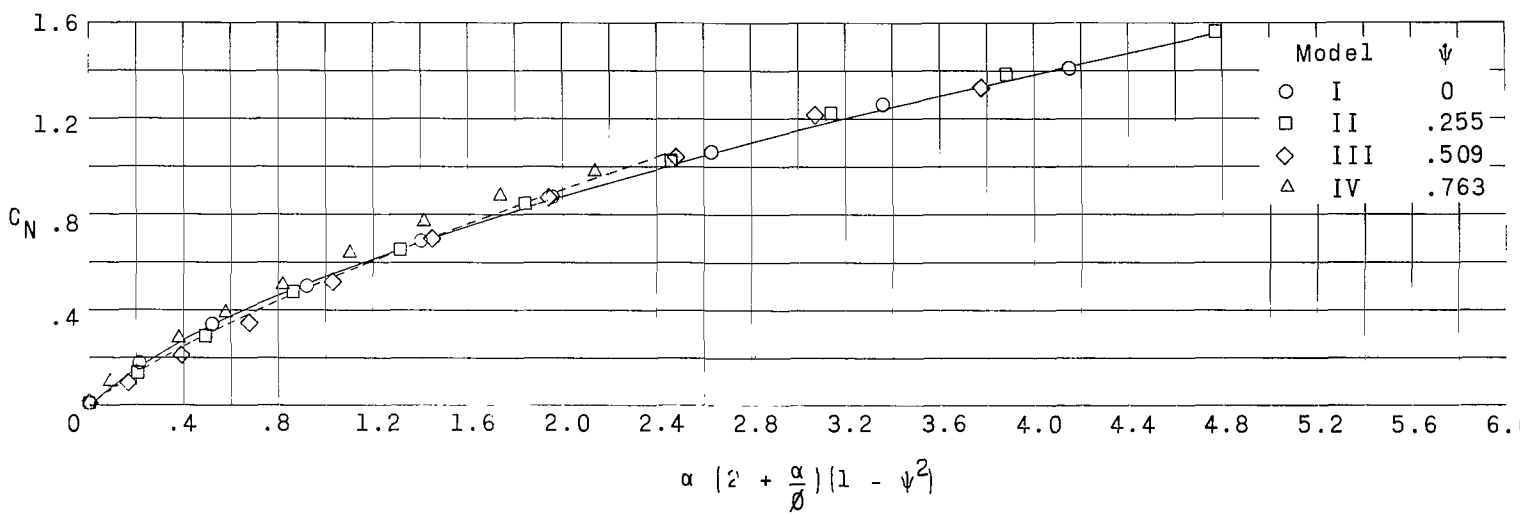

(b) Effect of bluntness ratio; $\phi = 10^{\circ}$.

Figure 10.- Normal-force-coefficient correlation for various bluntness ratios and cone angles.

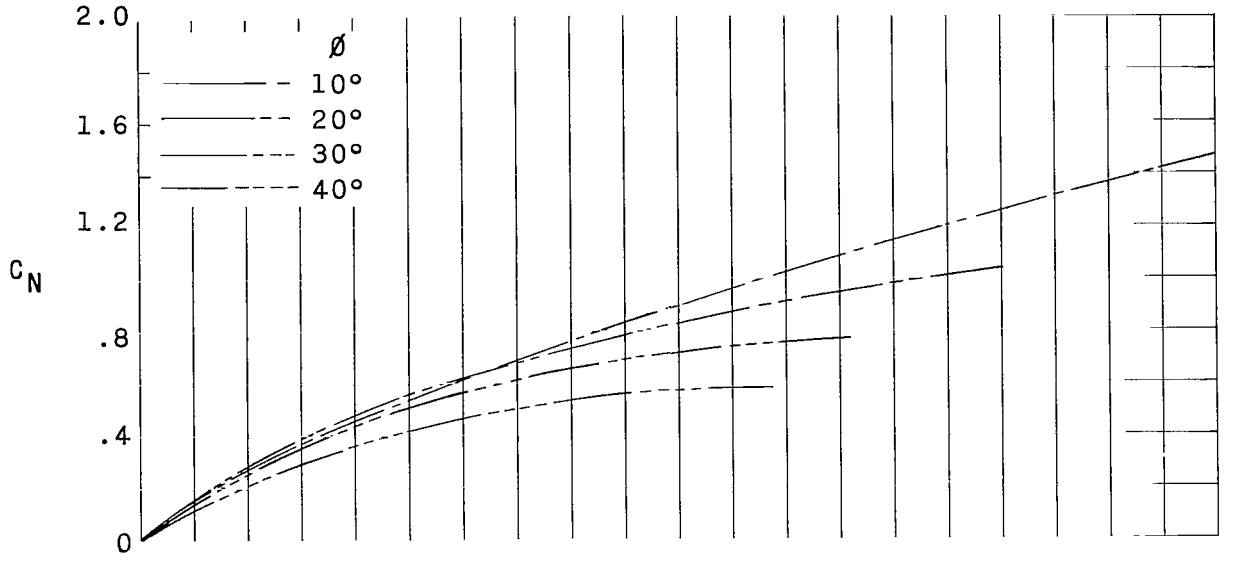

(a) Effect of increasing cone angle; $\psi = 0.2$.

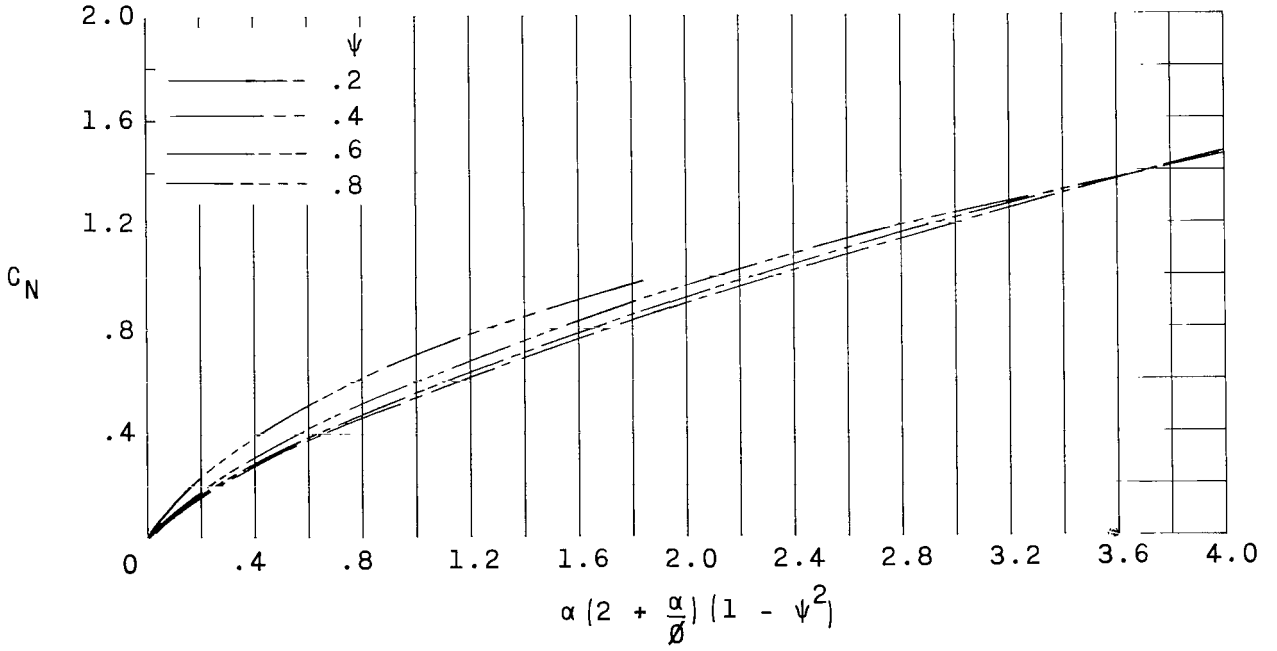

(b) Effect of increasing bluntness ratio; $\emptyset = 10^{\circ}$.

Figure 11.- Theoretical study of the parameter used in the normal-force-coefficient correlation.

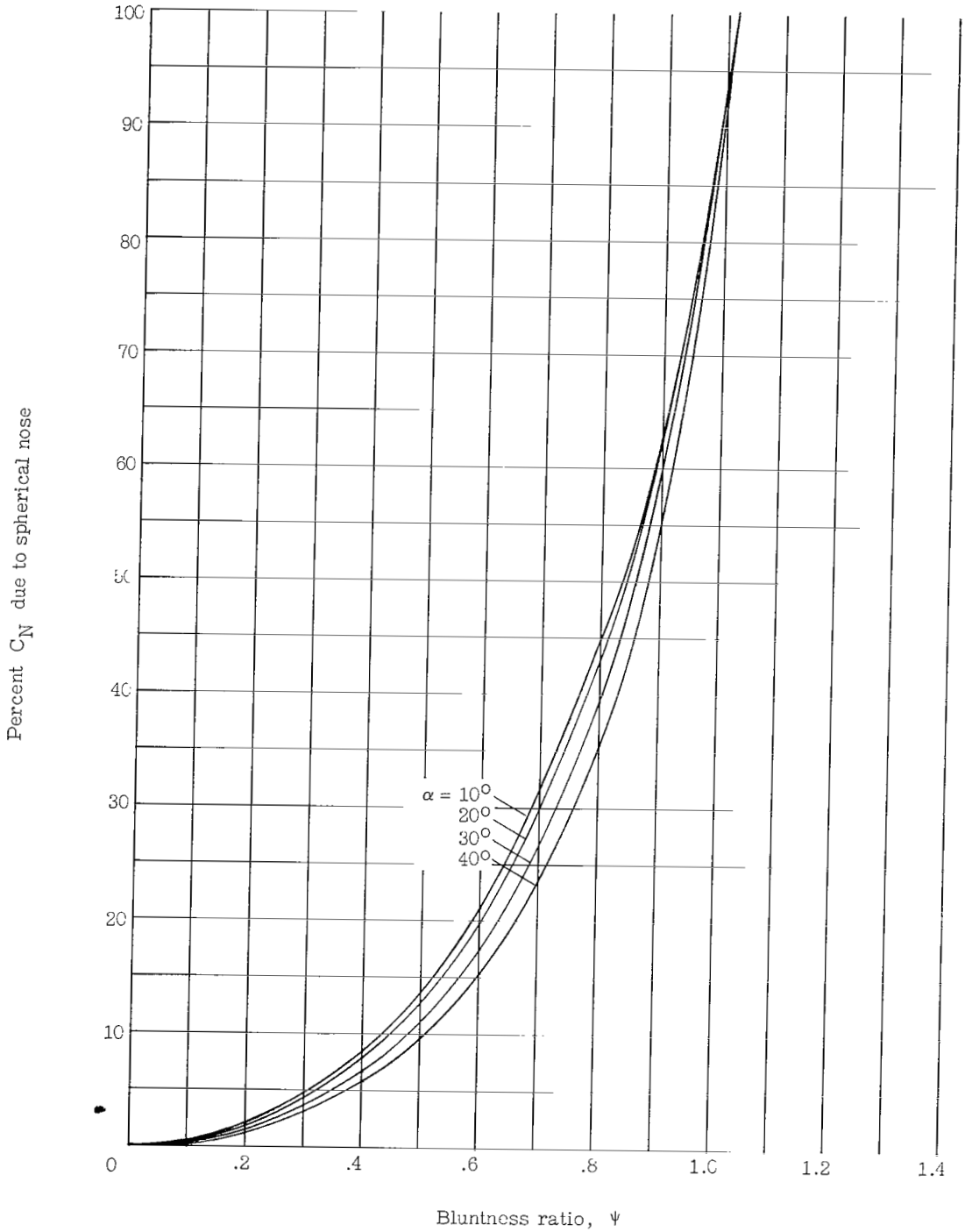

(a) $\phi = 10^{\circ}$.

Figure 12.- Percentage contribution of blunted cone normal-force coefficient due to spherical nose.

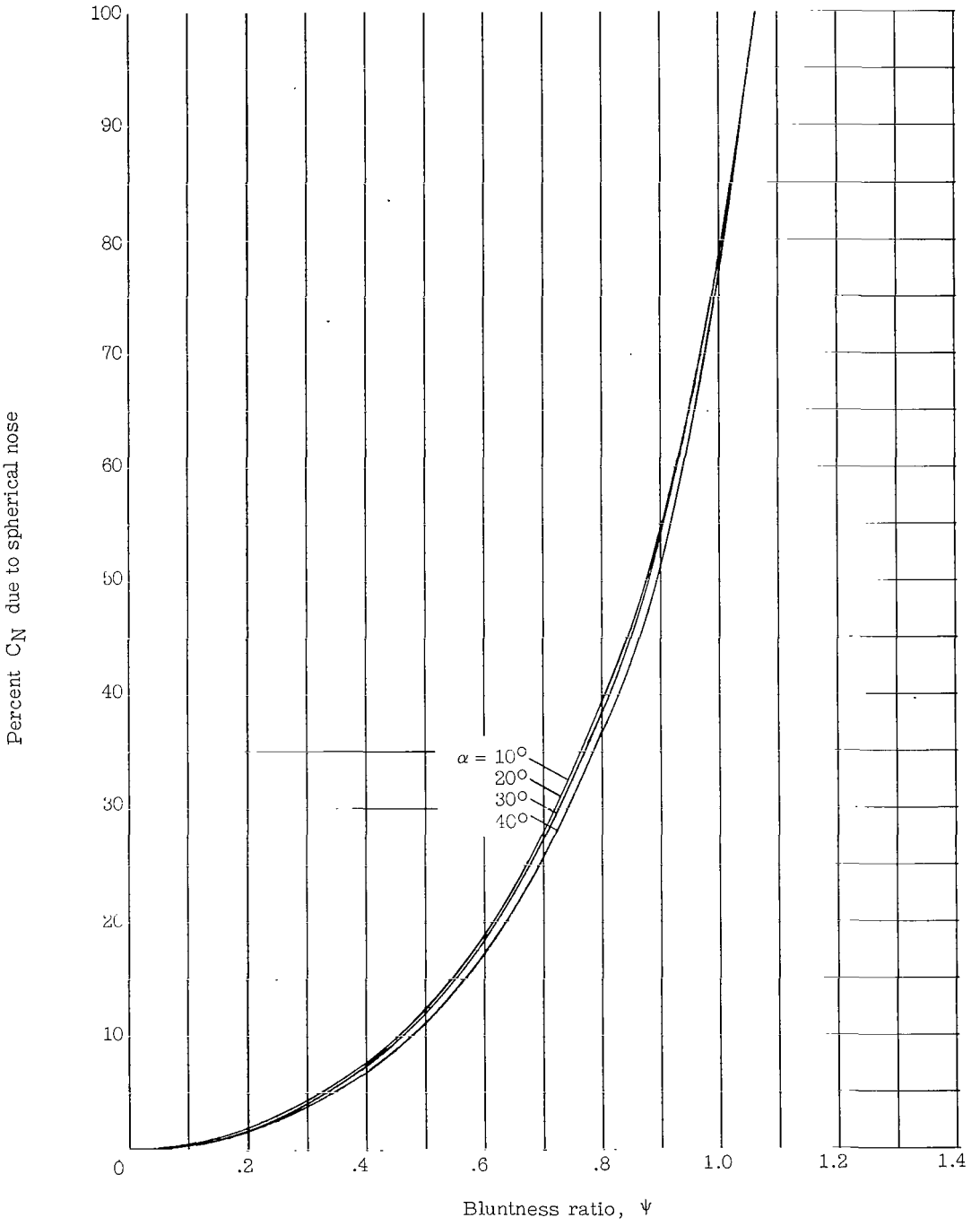

(b) ϕ = 20°.

Figure 12.- Continued.

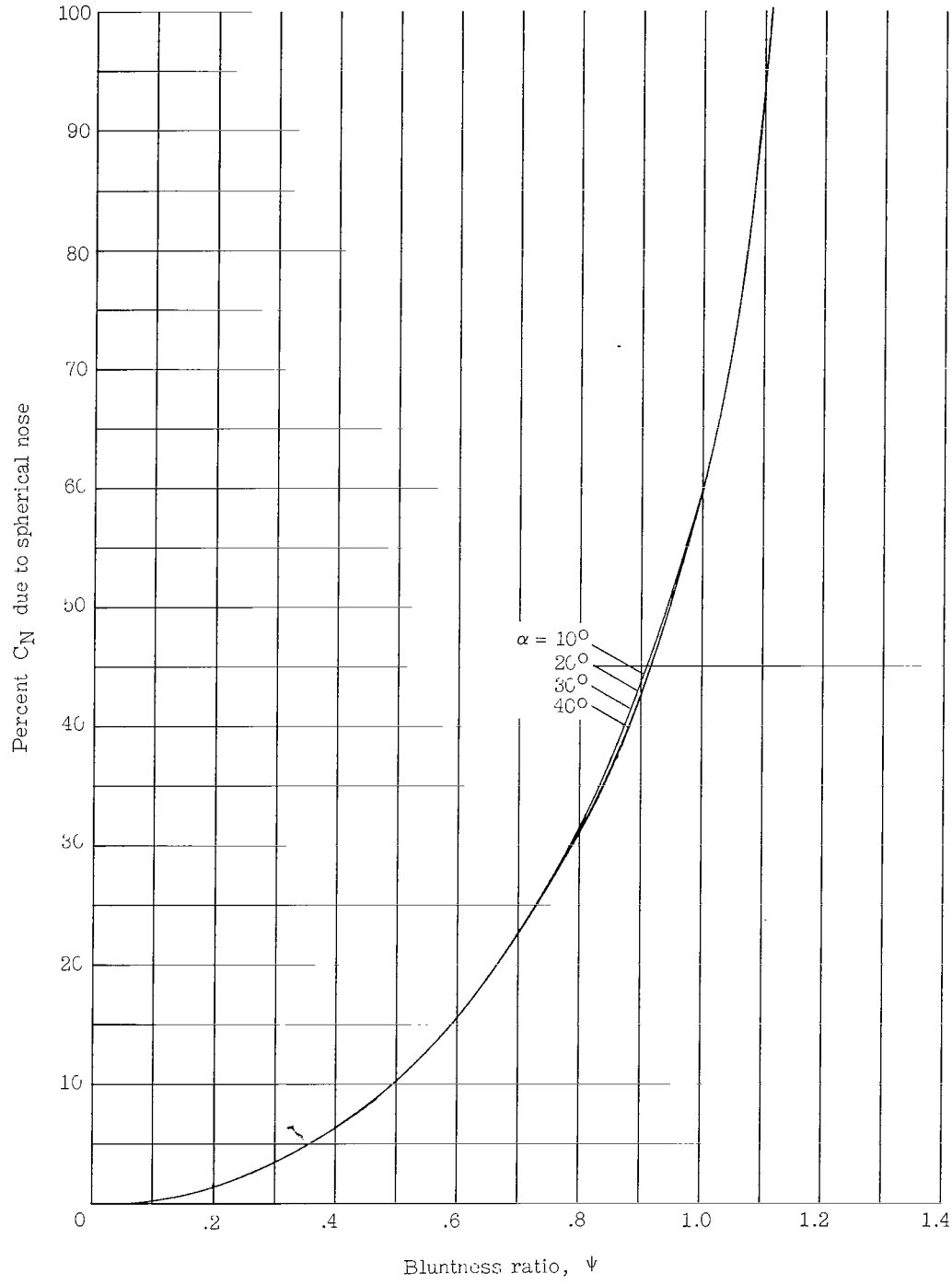

(c) $\phi = 30°$.

Figure 12.- Continued.

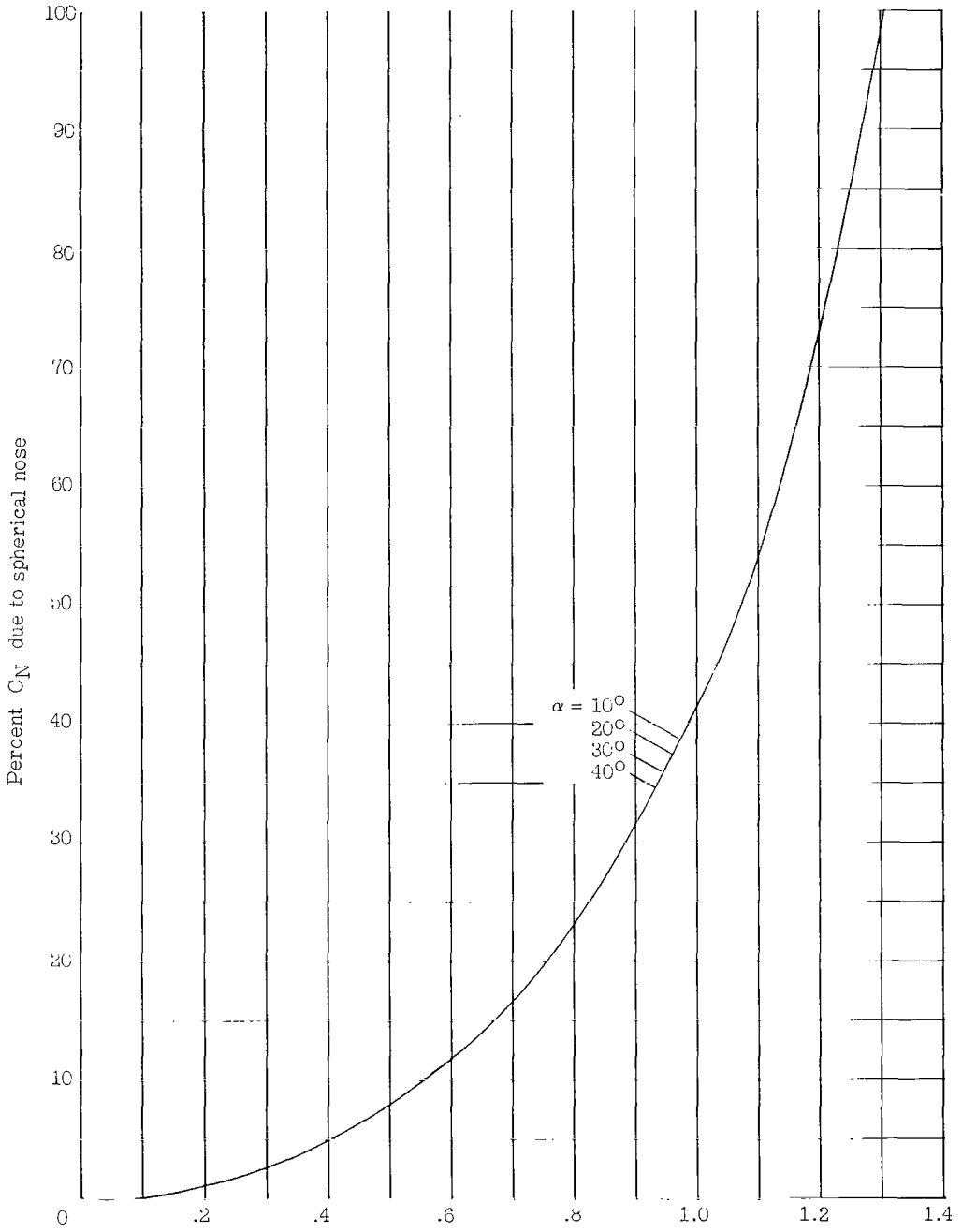

(d) $\phi = 40^\circ$.

Figure 12.- Concluded.

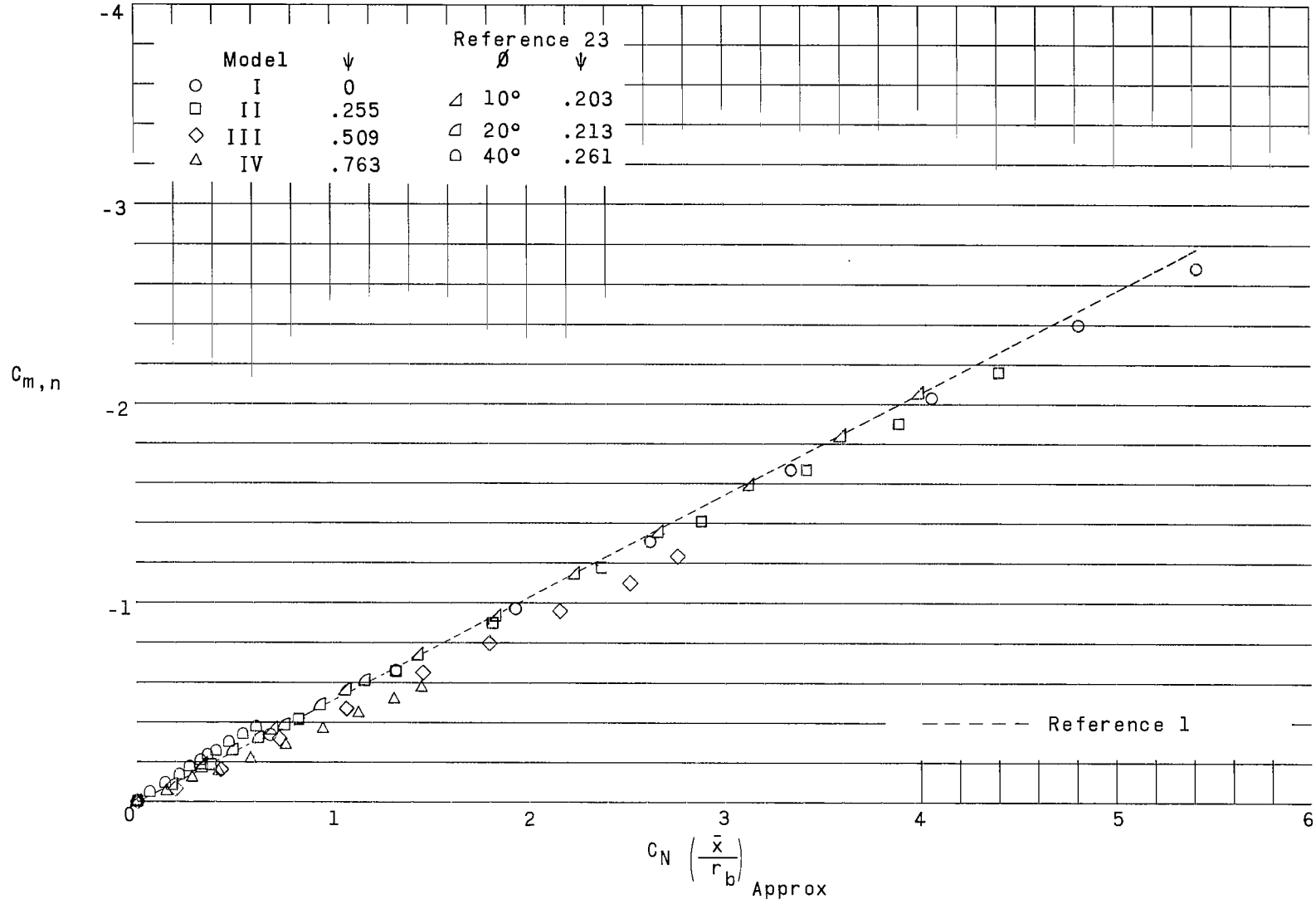

(a) Correlation based on approximate centroid location.

Figure 13.- Pitching-moment-coefficient correlation for cones with various cone angles and bluntness ratios.

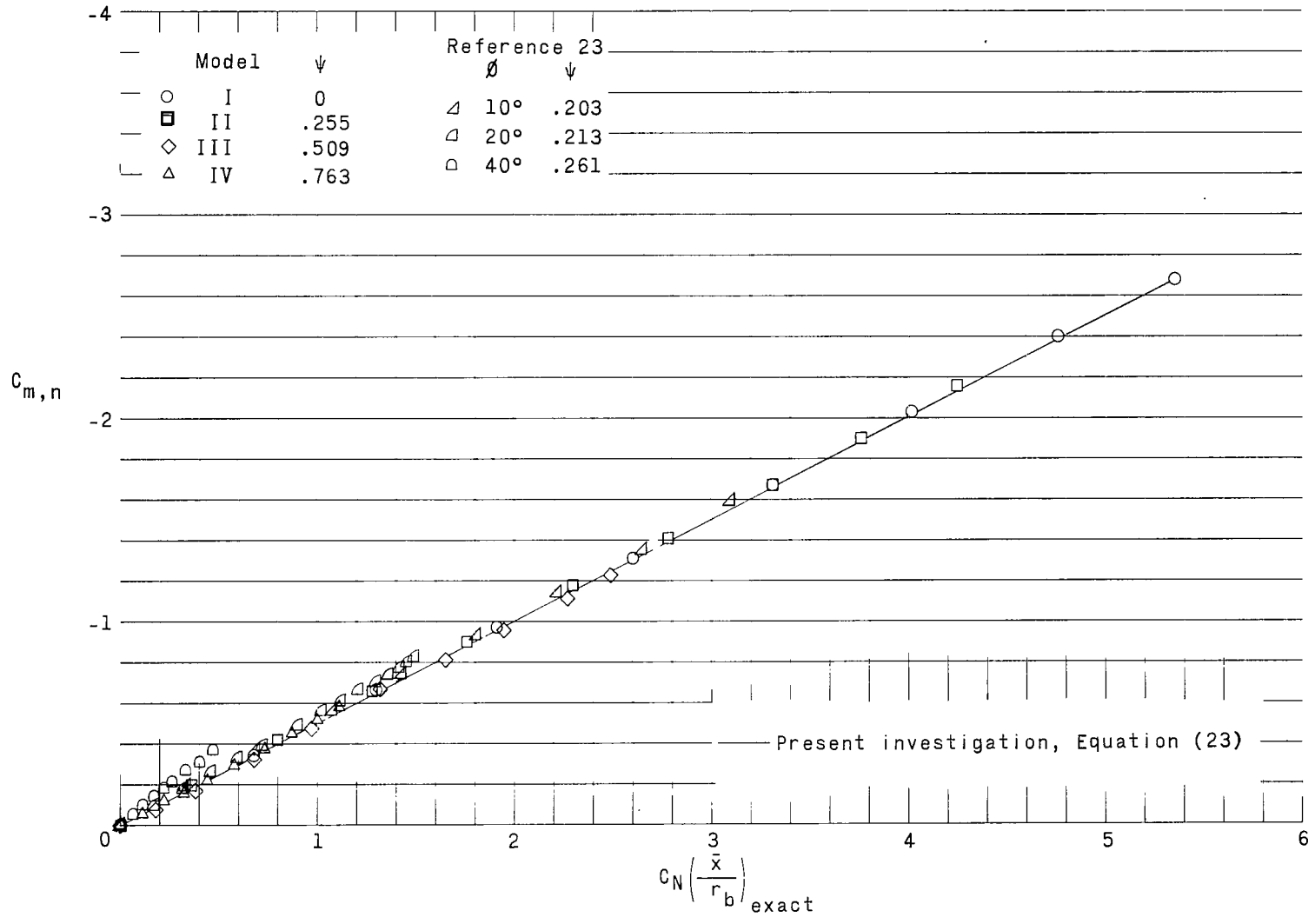

(b) Correlation based on exact centroid location.

Figure 13.- Concluded.

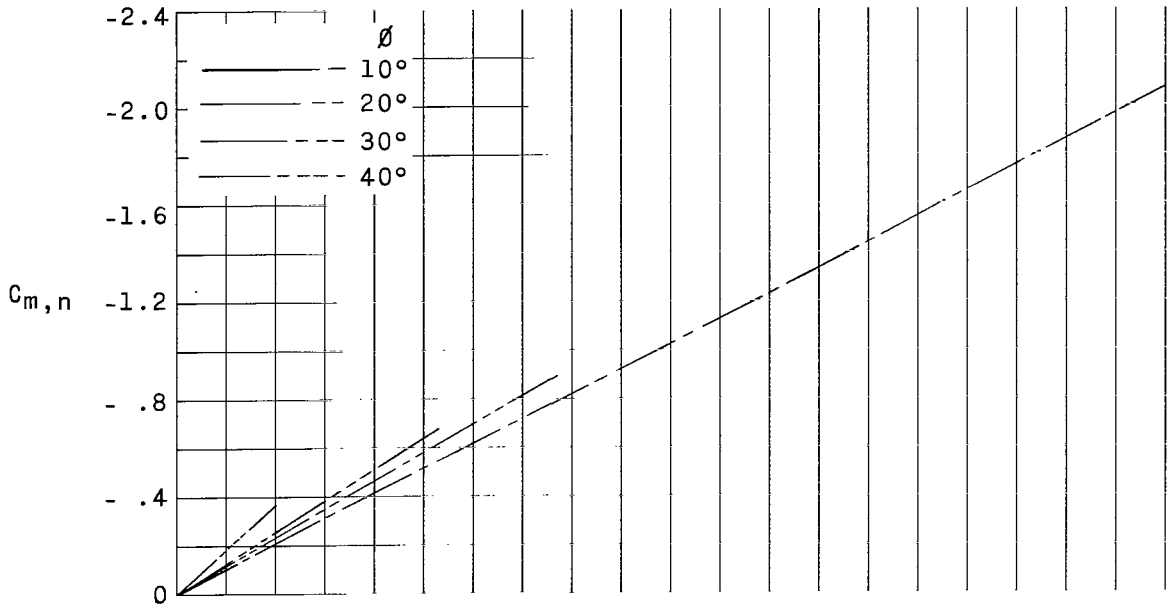

(a) Effect of cone angle; $\psi = 0.2$.

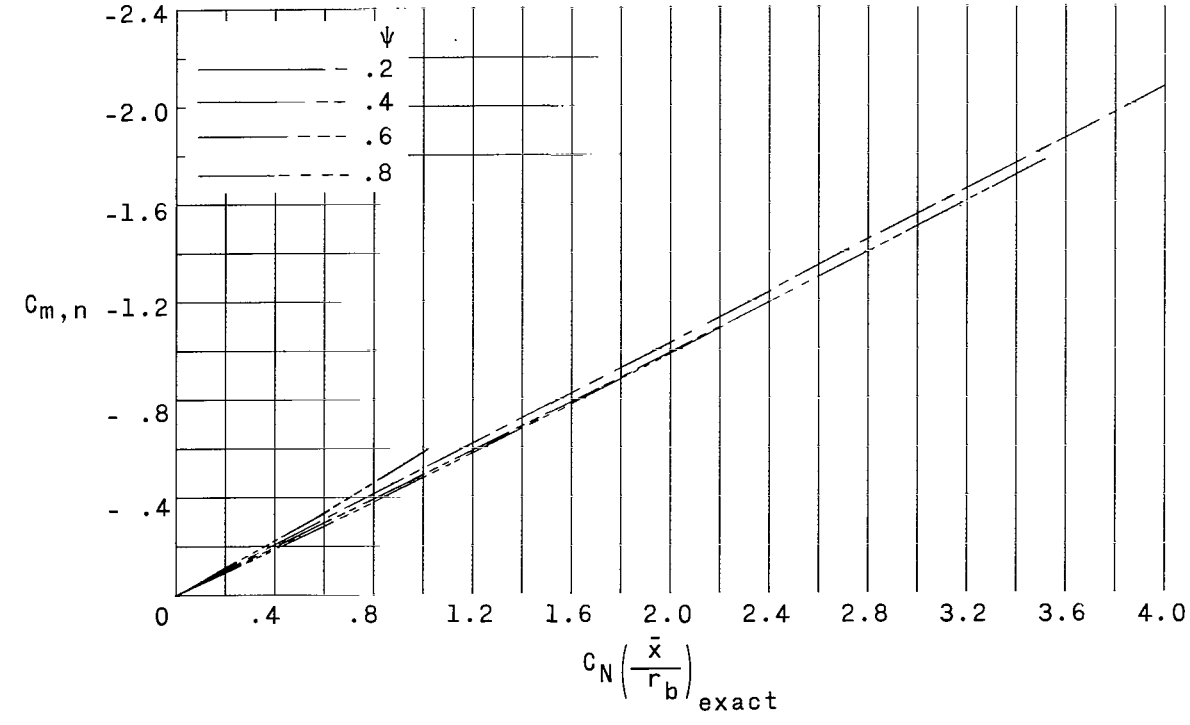

(b) Effect of bluntness ratio; $\emptyset = 10^\circ$.

Figure 14.- Theoretical study of parameter used in the pitching-moment-coefficient correlation.

2/7/25

"The aeronautical and space activities of the United States shall be conducted so as to contribute . . . to the expansion of human knowledge of phenomena in the atmosphere and space. The Administration shall provide for the widest practicable and appropriate dissemination of information concerning its activities and the results thereof."

—NATIONAL AERONAUTICS AND SPACE ACT OF 1958

NASA SCIENTIFIC AND TECHNICAL PUBLICATIONS

TECHNICAL REPORTS: Scientific and technical information considered important, complete, and a lasting contribution to existing knowledge.

TECHNICAL NOTES: Information less broad in scope but nevertheless of importance as a contribution to existing knowledge.

TECHNICAL MEMORANDUMS: Information receiving limited distribution because of preliminary data, security classification, or other reasons.

CONTRACTOR REPORTS: Technical information generated in connection with a NASA contract or grant and released under NASA auspices.

TECHNICAL TRANSLATIONS: Information published in a foreign language considered to merit NASA distribution in English.

TECHNICAL REPRINTS: Information derived from NASA activities and initially published in the form of journal articles.

SPECIAL PUBLICATIONS: Information derived from or of value to NASA activities but not necessarily reporting the results of individual NASA-programmed scientific efforts. Publications include conference proceedings, monographs, data compilations, handbooks, sourcebooks, and special bibliographies.

Details on the availability of these publications may be obtained from:

SCIENTIFIC AND TECHNICAL INFORMATION DIVISION

NATIONAL AERONAUTICS AND SPACE ADMINISTRATION

Washington, D.C. 20546